UNIVERSITÀ DEGLI STUDI DI PADOVA

DIPARTIMENTO DI FISICA E ASTRONOMIA "G. GALILEI"

CORSO DI LAUREA MAGISTRALE IN ASTRONOMIA

A geometric model for the off axis emission by short gamma ray bursts

Relatore:
Ch.mo Prof. Alessandro De Angelis

Candidato:
Andrea Garuffo
Matricola N. 1153688

Anno Accademico 2017/2018

CONTENTS

ABSTRACT

In this work I will present a model relating the flux emitted by a gamma-ray burst and the angle between the line of sight and the jet orientation, considering at first a homogeneous jet, then a more realistic structured jet with power law distribution of velocity and density. The model is based on the geometry of the phenomenon and not strictly dependent on the emission nature. Under the assumption of isotropic specific intensity, it is considered the emission by a sphere expanding at relativistic speed, then the region of interest is reduced to that of the cone defined by the jet aperture.
Inserting the parameters of the first peak of GRB170817A obtained by other works in the geometrical model resulted a not accurate fit of the light curve, but considering an angle of view of 0.35 the on axis equivalent luminosity obtained is $\sim 10^{51}$ erg s^{-1}, in agreement with the one derived in other works and also with the canonical luminosity of short gamma ray bursts.

1. INTRODUCTION

Gamma ray bursts (GRBs) are among the most energetic phenomena of the universe. These prompt emission of γ-rays are related to supernovae, black holes accretion and neutron stars merging, situated at cosmological distances and with a luminosity around 10^{51} erg s^{-1}, making them the most luminous objects in the sky.
The electromagnetic emission is produced by the interaction between the electrons of the material expelled at highly relativistic speed ($\Gamma \sim 50-100$), usually in two opposite collimated jets, and the extremely intense and turbulent magnetic field produced by the event. There are two possible scenarios that can explain the high energy gained by the electrons: internal and external shocks. For internal shock is intended the collision between two shells of ejected material: the outer and slower one is reached by a faster one creating a shock-wave that gives part of the energy to the electrons, accelerating them, and increases the density of the shocked material. In the external shock the collision is between the ejected material and the interstellar medium (ISM); then there is a lower density, because the ejecta are usually much denser than the ISM, but the difference in Lorentz factor between the two fronts is higher with respect to the previous case, in general $\Delta\Gamma \sim \Gamma_{ejecta}$ against $\Delta\Gamma \sim$ a few, thus producing a more violent collision.
These GRBs are expected to emit alongside electromagnetic waves also neutrinos and gravitational waves. In the last decades this kind of signal has been observed numerous times, even more than once a day, whereas gravitational waves and neutrinos have been observed only recently.
On August 17^{th} 2017 at 12:41:06.474598 UTC, for the first time ever, the joint emission of electromagnetic (GRB170817A) and gravitational waves (GW170817) compatible with the coalescence of two neutron stars was detected respectively by the Fermi Gamma-Ray Burst Monitor and the Advanced LIGO and Advanced Virgo detectors. The detection of this phenomenon, supposedly located in the galaxy NGC4993 at a distance of 42.9 ± 3.2 Mpc (Abbott et al. 2017), has extremely relevant implications for the study of GRBs: from the analysis of gravitational waves it is possible to gather information about the structure of the object generating the GRB and it showed an inclination angle θ_{obs} between the total angular momentum of the system and the line of sight (*los*) $\theta_{obs} \leq 36°$ or $\theta_{obs} \leq 28°$, if the value of the Hubble constant is assumed respectively $73.24 \pm 1.5 \mathrm{Kms}^{-1}\mathrm{Mpc}^{-1}$ (Riess et al. 2016) and $67.8 \pm 0.9 \mathrm{Kms}^{-1}\mathrm{Mpc}^{-1}$ (Planck collaboration 2016). It is impossible to extract this information from electromagnetic observations; so this occasion is fundamental in order to constraint the real energy involved in GRBs.
Although the complexity of the mechanism generating GRBs does not allow to create an exact model, it has been established with some certainty that they are related to the emission of narrow jets of relativistic matter, so the direction of the jet with respect to the *los* has effect on the observed flux, from which the isotropic equivalent energy is deducted; for this reason the information obtained by the gravitational waves are fundamental.
The emission of a GRB from the coalescence of two neutron stars is expected to happen within few seconds from the merging; the delay is due to the time necessary to the formation of the inner engine, to the acceleration of the jet material and the time of propagation of the photons

through the expelled material surrounding the inner engine. This prediction is reflected in the observed delay of $+1.74 \pm 0.05$ *s* between the detection of the first photons of GRB170817A and the peak of intensity of gravitational waves of GW170817 (Abbott et al 2017).
Further analysis of the gravitational wave data obtained by LIGO showed a descending signal starting ~ 0.67 s after the peak corresponding to the coalescence; this suggests that the newborn object is not, or at least not yet, a black hole, but the central engine of GRB170817A is likely a rotating hyper-massive neutron star (HMNS). This object is supposed to have mass $\sim 2.5\ M_{\odot}$ and radius ~ 16 Km; it avoids gravitational collapse thanks to rapid differential spinning and emits gravitational waves because it is still highly asymmetric; however it will eventually slow down and, after some delay, collapse into a stellar mass black hole. However, it is still not clear what this means with regard to GRB170817A: perhaps the first prompt emission is powered by the coalescence itself and related to the initial outflow from the HMNS while the second and softer emission is related to accretion of the orbiting debris on the later formed black hole (van Putten, Della Valle 2018).

1.1 GRB170817A

The light emitted by GRB170817A has been observed by many different observatories in many different wavelength, so the spectrum and light curve of the emission have been plenty analysed. For what concerns this work the data obtained by the Fermi Gamma-Ray Burst Monitor during the first few seconds since the detection are the most important. The duration of a GRB (T_{90}) is usually defined as the time between reaching the 5% and 95% of the cumulative observed fluence for the burst in the canonical energy range of $50-300$ keV; for GRB170817A was found $t_{90} = 2 \pm 0.5$ s, starting at T0 - 0.192 s, where T0$= 12:41:06.474598$ UTC on 2017 August 17. The first impulse, corresponding to the time interval between T0-0.320 s and T0$+0.256$ s, is best fitted by a Comptonized function with energy peak of $E_{peak} = 185 \pm 62$ keV and exponent $\alpha = -0.62 \pm 0.4$ (Goldstein et al. 2017); this results in a time-averaged flux of $(3.1 \pm 0.7) \times 10^{-7}$ erg s^{-1} cm^{-2} in the energy range from 10 KeV to 1 MeV (Abbott et al 2017). The main pulse is followed by a softer one lasting from $T0 + 0.832$ s to $T0 + 1.984$ s, which is well fitted by a black body with temperature $kT = 10.3 \pm 1.5$ Kev and has a mean flux, in the range $10-1000$ Kev, of $(0.53 \pm 0.1) \times 10^{-7}$ erg s^{-1} cm^{-2}; but the energy emission is close to the lower bound of the Fermi-GBM so it is not possible to exclude non thermal spectrum (Abbott et al. 2017). The softer emission is maybe related to the formation of a cocoon due to the transfer of energy from the jet to the surrounding dense material ejected during the coalescence. This cocoon is expanding at mildly relativistic speed with Lorentz factor $\Gamma_{cc} \approx 10$, much slower than the jet with $\Gamma \approx 50-100$ and has a much wider opening angle with respect to the jet, thus the cocoon emission can be considered almost isotropic and it will not depend strongly on the angle of view.
The minimum variability time scale Δt_{min} is the time scale related to the rise time of the shortest pulse observed; on different energy ranges different values were found:

$$10-1000\ Kev \ \rightarrow \ \Delta t_{min} = 0.125 \pm 0.064 \text{ s} \tag{1.1}$$

$$10-50\ Kev \ \rightarrow \ \Delta t_{min} = 0.312 \pm 0.065 \text{ s} \tag{1.2}$$

$$10-300\ Kev \ \rightarrow \ \Delta t_{min} = 0.373 \pm 0.069 \text{ s}. \tag{1.3}$$

There is a relation between the hardness of the pulse and the rise time scale; indeed as shown by Golkhou et al. (2015) to higher energy corresponds shorter pulses and this behaviour has been observed also in the emission of GRB170817A (Goldstein et al. 2017).
The shape of the pulses is described quite accurately by the equations:

$$I(t) = A\,exp\Big(-\Big(\frac{t_{peak}-t}{\sigma_{rise}}\Big)^{\nu}\Big) \quad for\ t \leq t_{peak} \tag{1.4}$$

$$I(t) = A\,exp\Big(-\Big(\frac{t-t_{peak}}{\sigma_{decay}}\Big)^{\nu}\Big) \quad for\ t \geq t_{peak} \tag{1.5}$$

where A is the amplitude of the pulse and t_{peak}, σ_{rise}, σ_{decay} are the characteristic time scales of the rise and decay (Norris et al. 2005). For GRB170817A has been found:

$$t_{peak} = -114 \pm 45 \text{ ms} \quad \sigma_{rise} = 129 \pm 45 \text{ ms} \quad \sigma_{decay} = 306 \pm 64 \text{ ms} \quad \nu \approx 2 \tag{1.6}$$

where the start time of the pulse is $t_{10} = T0 - 0.310 \pm 0.048$ s, defined as the time at which the pulse reaches 10% of the maximum amplitude (Goldstein et al. 2017). The rising time is equated to the minimum variability time scale that can be attributed to the light-crossing time of the individual emission regions and is expressed as:

$$\sigma_{rise} \approx \frac{\delta R}{2c\Gamma^2} \tag{1.7}$$

where δR is the thickness of the emission region. The decay time is attributed to angular effects and is defined as:

$$\sigma_{decay} = \frac{R(1-\cos(\theta_{obs}-\theta_e))}{c} \approx \frac{R}{2c\Gamma^2} \tag{1.8}$$

where R is the radius of the shell, θ_e is the angle of emission of the photon and the approximation is valid if it is assumed that the solid angle accessible to the observer is limited by relativistic beaming. In the scenario of internal shock, assuming a Lorentz factor < 100 for the outer and slower shell and that the whole time delay between GW and GRB is due to jet propagation, given the measured time scales (eqns. 1.6) it results for $\Gamma = 100$ (Abbot et al 2017)

$$R \sim 2 \times 10^{14}\text{cm} \quad \delta R \sim 7 \times 10^{13}\text{cm}. \tag{1.9}$$

Whereas, considering the softer thermal signal, it could be related to the emission of the photosphere of the fireball before it becomes optically thin to γ-rays. In this case the delay between GW and GRB is possibly due to the time necessary to the photosphere to expand enough to become optically thin. This leads to other possible values for the distance from the inner engine at which the radiation is emitted, corresponding to the photosphere's radius: the smaller one is the innermost stable circular orbit of a Schwarzchild black hole with mass equal to the stimated inner engine mass $M_{BH} = 2.8\,M_{\odot}$ and the greater is obtained from the expression proposed by

Nakar and Sari 2012:

$$R = 1.4 \times 10^9 \left(\frac{t}{1\ \mathrm{s}}\right)\left(\frac{T}{10\ \mathrm{keV}}\right)^2 \mathrm{cm} \tag{1.10}$$

with the results 2.5×10^6 cm $< R < 3 \times 10^8$ cm (Abbot 2017).
From the collected data it has been deducted that GRB170817A is strangely dim: with an isotropic equivalent energy of $E_{iso} = 4.17^{+6.54}_{-0.99} \times 10^{46}$ erg is many order of magnitude less energetic than the usual sGRB (Zhang et al 2018).
There are two main possibilities to produce a low luminosity sGRB from a neutron star merger. The first one is a usually bright sGRB jet viewed off-axis; within this picture, the main jet is directed toward a different direction with respect to the observer. In a similar scenario, a uniform conical jet is disfavoured because, due to relativistic beaming, the radiation emitted by a source moving at high speed it is unlikely to be viewed outside the jet cone. A more promising scenario is a structured jet, still viewed from off axis with respect to the central and faster region; in this case the observed emission is from the slower outer regions with low luminosity along line of sight. The extreme case of a structured jet is a cocoon: a really wide outflow of material at mildly relativistic speed expanding almost spherically, maybe produced by the interaction of an original collimated jet with the surrounding dense environment.
The second possibility is that GRB 170817A may be intrinsically low energetic. However, the late rise of X-ray and radio flux from the source suggests that the total energy budget is higher, disfavouring this possibility in favour the off-axis structured jet scenario.

2. MODEL

2.1 Dynamics' effects on emission

Due to the high speed of the particles it is necessary to calculate the relativistic effects that their motion has on the emitted radiation. Consider the rest frame F' in which the particle has zero velocity, since charged particles have to be accelerated in order to emit radiation F' is inertial with respect to the source only at a given time t and in an infinitesimal neighbourhood of t the motion is still not relativistic. Suppose that in such frame a energy dW' is emitted in the interval dt', due to how F' is defined the motion is non-relativistic then the emission is isotropic and has vanishing momentum $dp' = 0$. In the observer reference frame the source is moving at speed $-v$ and, given the definition of the Lorentz factor $\gamma = (1-(v/c)^2)^{-1/2}$, it is seen emitting energy

$$dW = \gamma\, dW' \tag{2.1}$$

since energy and momentum form a 4-vector. The time interval transforms as

$$dt = \gamma\, dt' \tag{2.2}$$

then the total emitted power is:

$$P' = \frac{dW'}{dt'} \qquad P = \frac{dW}{dt} \tag{2.3}$$

this means that $P = P'$ or that the total emitted power is Lorentz invariant.
The radiation emitted by a non-relativistic source is given by the Larmor formula:

$$|E_{rad}| = |B_{rad}| = \frac{q_e \dot{v}}{Rc^2} \sin\Phi \tag{2.4}$$

where $\dot{v}$ is the acceleration of the charge and Φ the angle between the direction $\hat{n}$ of the emission; the resulting Poynting vector is

$$S = \frac{c}{4\,\pi} E_{rad}^2 = \frac{q_e^2\, \dot{v}^2}{4\,\pi\, R^2\, c^3} \sin^2\Phi. \tag{2.5}$$

The energy emitted per unit solid angle $d\Omega$ per unit time dt around $\hat{n}$ is

$$\frac{dW}{dt} = S \cdot R^2\, d\Omega \tag{2.6}$$

then

$$\frac{dW}{dt\,d\Omega} = \frac{q_e^2\,\dot{v}^2}{4\,\pi\,c^3}\sin^2\Phi \tag{2.7}$$

integration over the solid angle to consider all the direction of emission results:

$$P = \frac{dW}{dt} = \frac{q_e^2\,\dot{v}^2}{4\,\pi\,c^3}\int_{4\pi}\sin^2\Phi d\Omega \tag{2.8}$$

that is the Larmor formula for a single accelerated particle:

$$P = \frac{2\,q_e^2\,\dot{v}^2}{3\,c^3} = \frac{2\,q_e^2}{3\,c^3}|a'|^2. \tag{2.9}$$

Since 4-velocity and 4-acceleration are orthogonal ($a'^{\alpha}\cdot v'^{\alpha}=0$), in the rest frame F' $v'^{\alpha} = (c,0,0,0)$ and $a' = \dot{v}'$, then $a'_0 = 0$; thus

$$|a'|^2 = \sum_{k=1}^{3} a_k \cdot a^k = \vec{a}\cdot\vec{a} \tag{2.10}$$

and finally the total emitted power is

$$P = \frac{2\,q_e^2}{3\,c^3}\,\vec{a}\cdot\vec{a}. \tag{2.11}$$

However in this way the dependence on the angle disappears, whereas it is important for what concerns GRBs. The solid angle is defined in the two reference frame as

$$d\Omega = d\mu\;d\varphi \qquad d\Omega' = d\mu'\;d\varphi' \tag{2.12}$$

where $d\mu = \sin\theta\;d\theta$ and $d\mu' = \sin\theta'\;d\theta'$, and since energy and momentum form the 4-vector

$$dW^{\alpha} = \gamma(dW' + \vec{v}dp') = \gamma(1-\beta\mu)\,dW' \tag{2.13}$$

where $\beta = v/c$; then, given $d\varphi = d\varphi'$, the following relations hold:

$$\mu = \frac{\mu'+\beta}{1+\beta\mu'} \quad\rightarrow\quad d\mu = \frac{d\mu'}{\gamma^2\,(1+\beta\mu')^2} \tag{2.14}$$

$$d\Omega = \frac{d\Omega'}{\gamma^2\,(1+\beta\mu')^2} \tag{2.15}$$

and finally

$$\frac{dW}{d\Omega} = \gamma^3\,(1+\beta\mu)^3\frac{dW'}{d\Omega'} \tag{2.16}$$

Now, it is necessary to distinguish between emitted and received power from the point of view of the observer, respectively P_e and P_r: the first is obtained considering the interval of time during which the radiation is emitted $dt = \gamma dt'$, the latter considering the interval of time during which the radiation is received $dt = \gamma(1+\beta\mu)\,dt'$; then

$$\frac{dP_e}{d\Omega} = \gamma^2\,(1+\beta\mu)^3\frac{dP'}{d\Omega'} = \frac{1}{\gamma^4\,(1-\beta\mu)^3}\frac{dP'}{d\Omega'} \tag{2.17}$$

$$\frac{dP_r}{d\Omega} = \gamma^4\,(1+\beta\mu)^4\frac{dP'}{d\Omega'} = \frac{1}{\gamma^4\,(1-\beta\mu)^4}\frac{dP'}{d\Omega'}. \tag{2.18}$$

The interesting one is P_r, which is the effective power received by the observer; thus from eqn. 2.9

$$\frac{dP'}{d\Omega'} = \frac{q_e\,(a')^2}{4\,\pi\,c^3}\sin^2\phi' \tag{2.19}$$

which is usually not easy to calculate due to the unknown angle, except for two specific cases. When, in the rest frame, the velocity and acceleration are parallel:

$$\Phi' = \theta \quad\rightarrow\quad \sin^2\theta' = \frac{\sin^2\theta}{\gamma^2\,(1-\beta\mu)^2} \tag{2.20}$$

then

$$\frac{dP_\parallel}{d\Omega} = \frac{q_e^2 a_\parallel^2}{4\,\pi\,c^3}\,\frac{\sin^2\theta}{(1-\beta\mu)^6}. \tag{2.21}$$

When they are perpendicular:

$$\cos\Phi' = \sin\theta'\cos\varphi' \quad\rightarrow\quad \sin^2\Phi' = 1 - \frac{\sin^2\theta\cos^2\varphi}{\gamma^2(1-\beta\mu)^2} \tag{2.22}$$

resulting in

$$\frac{dP_\perp}{d\Omega} = \frac{q_e^2 a_\perp^2}{4\,\pi\,c^3}\,\Big[1 - \frac{\sin^2\theta\cos^2\varphi}{\gamma^2(1-\beta\mu)^2}\Big]. \tag{2.23}$$

In the case of highly relativistic ($\gamma \gg 1$) sources holds the approximation:

$$(1-\beta\mu) \approx \frac{1+\gamma^2\theta^2}{2\gamma^2} \tag{2.24}$$

then the power received per solid angle can be approximated as

$$\frac{dP_\parallel}{d\Omega} \approx \frac{16\,q_e^2 a_\parallel^2}{\pi\,c^3}\,\gamma^{10}\,\frac{\gamma^2\theta^2}{(1+\gamma^2\theta^2)^6} \tag{2.25}$$

$$\frac{dP_\perp}{d\Omega} \approx \frac{4\,q_e^2 a_\perp^2}{\pi\,c^3}\,\gamma^8\,\frac{1-2\gamma^2\theta^2\cos 2\varphi + \gamma^4\theta^4}{(1+\gamma^2\theta^2)^6} \tag{2.26}$$

in which the dependence on θ appears through the term $\gamma\theta$ and there is a maximum in the emission for $\theta \sim 1/\gamma$. It means that, since $\gamma \gg 1$ was considered, most of the emission is concentrated in a cone of half opening $\sim 1/\gamma$ around the direction of the motion.
It is a good approximation to assume that most of the emission of a relativistic jet is due to synchrotron radiation. The power emitted via synchrotron for unit frequency by electrons with power law energy distribution, moving at relativistic speed with Lorentz factor Γ is, in the source rest frame:

$$P'_{\nu'} = \frac{\sqrt{3}q^3 K B' \sin\eta}{m_e c^2 (p+1)} \Gamma\left(\frac{p}{4}+\frac{19}{12}\right)\Gamma\left(\frac{p}{4}-\frac{1}{12}\right)\left(\frac{m_e c \nu'}{3qB\sin\eta}\right)^{(1-p)/2} \tag{2.27}$$

$$K = (p-1) n_0 \gamma_{e,min}^{p-1} \tag{2.28}$$

where η is the angle between the magnetic field B' and the electron velocity, γ_{min} is the minimum Lorentz factor of the electrons in the rest frame of the distribution which has numeric density n_0. Given a power law energy distribution of the electron, delimited by the maximum electrons Lorentz factor $\gamma_{e,max}$ obtained equating the acceleration time and the energy loss time (de Jager et al. 1996) and by $\gamma_{e,min}$, for $1 < p < 2$ are defined as

$$N(E)dE = E^{-p}dE \tag{2.29}$$

$$\gamma_{e,max} \sim 4 \times 10^7 B'^{-1/2} \tag{2.30}$$

$$\gamma_{e,min} = \left[\frac{2-p}{p-1}\frac{m_p}{m_e}\varepsilon_e \Gamma \gamma_{e,max}^{p-2}\right]^{1/(p-1)} \tag{2.31}$$

where m_p is the proton mass and $\varepsilon_e \sim 0.1$ is the fraction of internal energy given to the electrons. In general the approximation

$$\gamma_e \approx \langle\gamma_e\rangle \frac{(p-2)}{(p-1)} \tag{2.32}$$

is valid, with $\langle\gamma_e\rangle$ the mean value of γ_e.
Assumed that the specific intensity $I'_{\nu'}$ is isotropic in the source rest frame and given

$$dP'_{\nu'} = \frac{I'_{\nu'}}{c} d\Omega \cos^2\theta \tag{2.33}$$

it follows

$$\begin{aligned} P'_{\nu'} &= \int_{4\pi} dP'_{\nu'} = \frac{1}{c}\int_{4\pi} I'_{\nu'}\cos^2\theta d\Omega \\ &= \frac{I'_{\nu'}}{c}\int_0^{2\pi} d\phi \int_{-1}^{1} \mu^2 d\mu = \frac{4\pi I'_{\nu'}}{3c}. \end{aligned} \tag{2.34}$$

Assuming that the prompt emission happens in the outer region of the source, so radiation is

not absorbed by other ejected material and neglecting intergalactic and galactic absorption and scattering (weak hypothesis, useful only for upper limit), in other words propagation in the void; it yields:

$$\frac{dI'_{\nu'}}{ds} = 0 \;\rightarrow\; I'_{\nu'} = const. \tag{2.35}$$

Given this hypothesis the flux for unit frequency is:

$$F'_{\nu'} = \int_{S(t)} I'_{\nu'} \cos\alpha \, d\Omega = \int_{S(t)} \frac{3\,c\,P'_{\nu'}}{4\pi} \cos\alpha \, d\Omega \tag{2.36}$$

for compact sources $\cos\alpha \approx 1$ is a good approximation, through the Doppler factor $\Lambda(\theta)$ the quantity is expressed in the observer rest frame:

$$F_\nu = \frac{3\,c\,P'_{\nu'}}{4\pi} \int_{S(t)} \Lambda^3 \, d\Omega \tag{2.37}$$

$$\Lambda(\theta) = [\Gamma(1-\beta\cos\theta)]^{-1}. \tag{2.38}$$

A more realistic scenario includes also synchrotron self-absorption; it is usually negligible, specially in the γ-ray range, but has to be considered for frequencies in the soft X-ray range.
The optical depth is to be known in order to estimated the effects of self absorption; it can be approximated as $\alpha'_{\nu'} R/\Gamma$, where

$$\alpha'_{\nu'} = \frac{p+2}{8\pi m_e (\nu')^2} \int_{\gamma_{min}}^{\infty} P'_{\nu',e}(\gamma_e) \frac{N(\gamma_e)}{\gamma_e} \, d\gamma_e. \tag{2.39}$$

Then the radiative transport equation has to be modified to include absorption in the case $\alpha'_{\nu'} R/\Gamma \sim 1$:

$$\frac{dI'_\nu}{ds} = I'_{\nu'}(1-\alpha'_{\nu'}) \tag{2.40}$$

thus leading to a decrease in intensity as the distance increases.

In the following sections will be presented the model representing the effect of off axis view of the emission from a pulse on the observed flux, developed using only geometrical properties and as few assumptions as possible on the emission.

2.2 Expanding sphere

In order to produce a simple model to represent the emission from an off axis jet, I first considered a spherical shell with negligible thickness, radius r and expanding at relativistic speed

with a Lorentz factor Γ. Given $I(x,t)$, the specific intensity of the single surface element, the bolometric flux emitted by the sphere is

$$F(t) = \int_{S(t)} I(x,t) \cos\alpha \frac{dS}{s^2} \tag{2.41}$$

where $S(t)$ is the locus of points on the surface of the sphere with equal arrival time t to the observer at cosmological distance D from the centre of the sphere. Assuming cylindrical symmetry with respect to the jet axis $dS = 2\pi r(t_e)^2 \sin\theta \, d\theta$ with $t_e = t - r/c$ the emission time; $s = D - r(t_e)\cos^2\theta$ is the distance between the element with coordinates (θ, ϕ, t_e) and the observer. Due to the cosmological distance and the small angular size of the source $cos\alpha \approx 1$; the result is:

$$F(t) = 2\pi \int_{S(t)} I(x,t) \frac{r^2(t)}{(D - r(t)\cos\theta)^2} \sin\theta \, d\theta. \tag{2.42}$$

For simplicity I assume constant luminosity during the pulse of duration T and isotropic emission in the rest frame of the source, thus the specific intensity has the general form:

$$I(x,t) = I(\theta)\left(\frac{r_0}{r(t)}\right)^2 \tag{2.43}$$

where $I(\theta)$ is related to the Doppler factor $\Lambda(\theta)$ due to the relativistic speed of the source:

$$I(\theta) = I'_0 \Lambda^{-4}(\theta) = I'_0 [\Gamma(1 - \beta\cos\theta)]^{-4}. \tag{2.44}$$

This assumption is justified if the emission is due to internal shocks which imply a constant number of emitting particles whose density decreases with the expansion of the sphere. In external shock scenarios such assumption may not be correct because during the expansion more particles are involved and then the emission may increase. So the flux emitted by the region $S(t)$ of the sphere is

$$F(t) = 2\pi I'_0 r^2 \int_{S(t)} \frac{\sin\theta \, d\theta}{(D - r(t)\cos\theta)^2 [\Gamma(1 - \beta\cos\theta)]^4} \tag{2.45}$$

where $'$ stands for the quantity in the source rest frame.

2.3 Off axis jet

In order to obtain the expression of the flux emitted by jet with semi-aperture θ_j and off axis by θ_{obs} with respect to the *los* of an observer situated along the z axis, as shown in figure (2.3) is enough to integrate over the region delimited by the jet. The region of integration depends on θ and then to time t: indeed, even if the whole surface emits at the exact same time, the first photon reaching the observer is the one emitted from the tip of the sphere along the *los*, then due to its large dimension of the source the observer will see the sequential lightning of concentric circles resulting from the intersection of the sphere with the plane $z = R\cos\theta$ moving in the $-z$ direction at the speed of light. Thus the time t at which the region of the jet nearest to the

observer turns on is related to the radius the jet inclination θ_{obs} and half-opening θ_j by:

$$\theta_{on} = \theta_{obs} - \theta_j \quad \rightarrow \quad \cos\theta_{on} = 1 - \frac{ct}{r} \tag{2.46}$$

and it will turn off at the end of the pulse with duration T. Analogously, the region turns off when it is reached by another plane moving at the same speed and in the same direction, but T later or cT behind of the previous. It is necessary to consider also the expansion of the sphere $\Delta r = c\beta T$ during the pulse: the effect of the shell expansion is to reduce the distance the light emitted at later times has to travel to the observer, thus also the difference of time of observation between first and last photon emitted is reduced. For this reason the factor $\tau = T(1-\beta)$ is introduced and the relation between time and jet characteristics is:

$$\theta_{off} = \theta_{obs} + \theta_j \quad \rightarrow \quad \cos\theta_{off} = 1 - \frac{c(t-\tau)}{r+\Delta r}. \tag{2.47}$$

Finally, substituting θ_{on} and θ_{off} in eqn. (2.5) as integration extrema results:

$$F(t) = 2\pi I'_0 r^2 \int_{\theta_{on}}^{\theta_{off}} \frac{\sin\theta\, d\theta}{(D - r(t)\cos\theta)^2 [\Gamma(1-\beta cos\theta)]^4}. \tag{2.48}$$

Expression 2.48 represents the flux emitted by the whole spherical crown delimited by θ_{on} and θ_{off}, not by the jet only, as shown in figure 2.1 and for $\theta_{obs} = 0$ reproduces the case of an on-axis jet. It is necessary to find the intersection between the previously mentioned planes and the jet to obtain the correct expression.

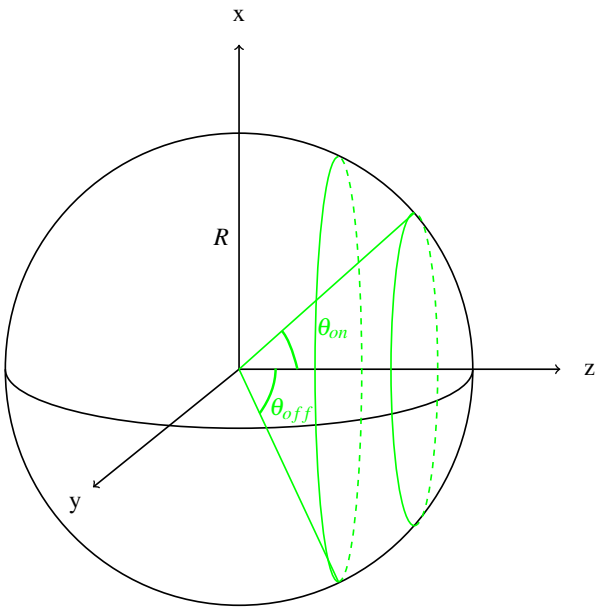

Fig. 2.1: Representative scheme for emitting spherical crown.

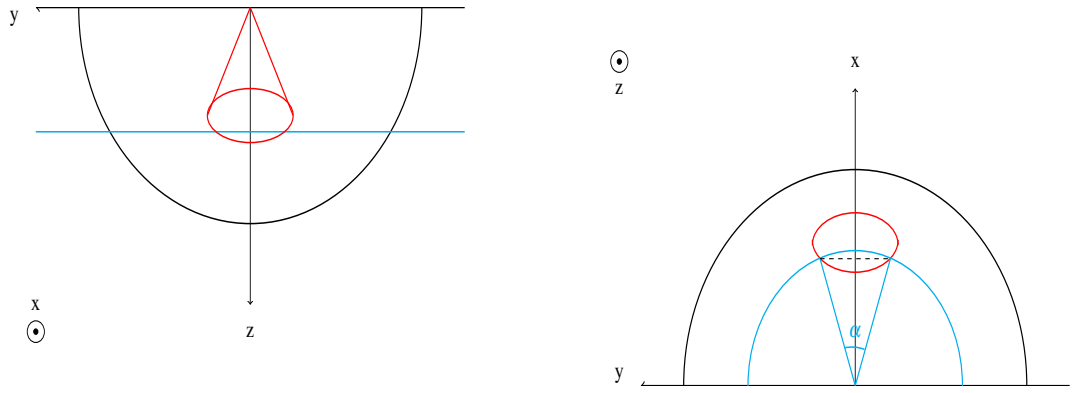

Fig. 2.2: Simplified top (left) and front (right) view of the representative scheme (fig. 2.3).

The locus of point of equal arrival time of photons to the observer on the z axis is a circumference defined by the intersection of the sphere with the plane $z = r cos\theta$, whereas if only the region delimited by the jet opening is emitting, then only an arc of circumference is emitting. Considering the two planes $z = r cos\theta$ and $z = r\cos(\theta + d\theta)$, their intersection with the sphere is a ring with radius $r\sin\theta$, height $d\theta$ and surface A_{ring}, the part of the ring delimited by the jet has surface A_{arc}; thus, due to the infinitesimal height of the ring the ratio between the surfaces is equal to the ratio between the length of arc and circumference. Moreover the flux is directly proportional to the emitting region, then

$$\frac{A_{arc}}{A_{ring}} = \frac{l_{arc}}{l_{ring}} \rightarrow \frac{F_{arc}}{F_{ring}} = \frac{l_{arc}}{l_{ring}} = \frac{l(\theta)}{2\pi r \sin\theta}. \tag{2.49}$$

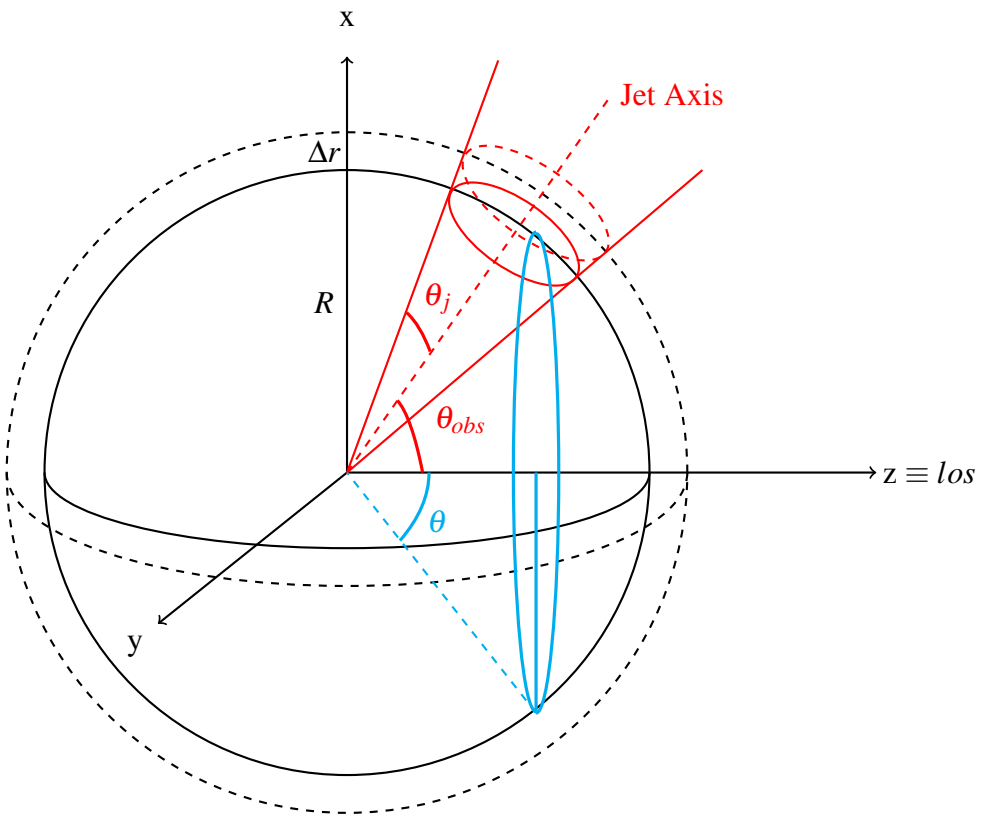

Fig. 2.3: Representative scheme of the expanding sphere (– and ––), the jet (–) and the causality plane (–).

By rotating the coordinate system counter-clockwise by θ_{obs} around y the jet axis overlaps the z' axis, then the emitting region of the jet is the smaller portion of the sphere delimited by the plane $z' = r\cos\theta_j$, ; thus the region of interest is the intersection of the planes:

$$z = r\,cos\theta \tag{2.50}$$

$$z' = z\,cos\theta_{obs} - x\sin\theta_{obs} = r\cos\theta_j \tag{2.51}$$

results

$$x = r\,\frac{\cos\theta_{obs}\,\cos\theta - \cos\theta_j}{\sin\theta_{obs}}. \tag{2.52}$$

It is also true that $x = r\sin\theta\,\cos\alpha$, so

$$\alpha = \arccos\left(\frac{\cos\theta_j - \cos\theta_{obs}\,\cos\theta}{\sin\theta_0\,\sin\theta}\right) \;\rightarrow\; l(\theta) = \alpha\, r\sin\theta. \tag{2.53}$$

Finally, the flux emitted by a jet with half opening θ_j seen off axis by an angle θ_{obs} is:

$$F(t) = 2I'_0 r^2 \int_{\theta_{off}}^{\theta_{on}} \arccos\left(\frac{\cos\theta_j - \cos\theta_{obs}\,\cos\theta}{\sin\theta_0\,\sin\theta}\right) \frac{\sin\theta\, d\theta}{(D - r(t)cos\theta)^2[\Gamma(1-\beta\cos\theta)]^4}. \tag{2.54}$$

Substituting the expression 2.34 of the specific intensity and approximating $D - r(t)cos\theta \approx D$, since the distance D of the source is much greater than its size, it results:

$$F(t) = \frac{3cP'r^2}{2\pi D^2} \int_{\theta_{off}}^{\theta_{on}} \arccos\left(\frac{\cos\theta_j - \cos\theta_{obs}\ \cos\theta}{\sin\theta_0\ \sin\theta}\right) \frac{\sin\theta\, d\theta}{[\Gamma(1-\beta\cos\theta)]^4}. \tag{2.55}$$

3. GEOMETRY EFFECTS

Lets assume, for the moment, that the emission is not dependent on any variable and pose

$$I'_0 = 1 \tag{3.1}$$

and focus on the effect of the structure itself on the emission in the hypothesis of uniform jet. Some relations linking the geometric characteristics to the flux arise from the model: for example, the time at which the first photon is seen is given by

$$t_{first} = \frac{r\,(1-\cos(\theta_{obs}-\theta_{jet}))}{c} \tag{3.2}$$

and the time at which the off-axis light curve reaches the maximum, just before the end of the emission, is

$$t_{peak,off} = \tau + \frac{(r+\Delta r)(1-\cos(\theta_{obs}-\theta_{jet}))}{c} \tag{3.3}$$

while for the on-axis one:

$$t_{peak,on} = \tau + \frac{(r+\Delta r)(1-\cos\theta_{jet})}{c} \tag{3.4}$$

However these are empirical relations and lose precision for some combinations of the parameters, see for example fig. 3.4, but the error is usually negligible if compared to the uncertainty introduced by the exposure time necessary to collect data, for example for Fermi GBM $t_{exp} \sim 0.1 - 0.05$ (Abbot et al. 2017).

3.1 Dependence on R

With regard to on axis emission, increasing the radius of the sphere, which represent the distance at which the emission happens, increases also the maximum of the flux and the duration of the observed emission, as shown in fig. 3.1. This is to be expected because an increase in radius means a quadratic increase of the emitting region and then of the flux. Also, a bigger source means that more time is required before the whole surface enters in causal contact with the observer, or in other words the delay between the observation of the first and last photons is greater for greater radii.

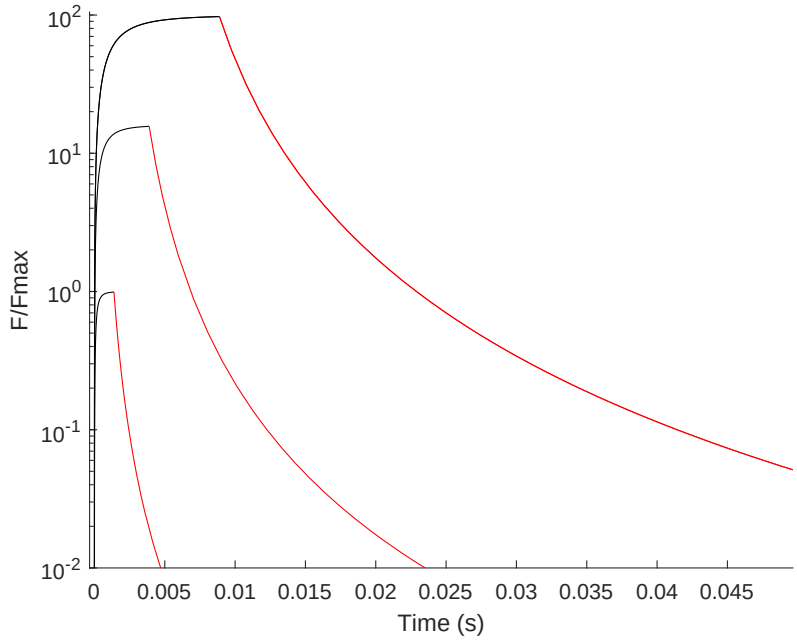

Fig. 3.1: On axis light curves for $R = 2 \times 10^{10} - 8 \times 10^{10} - 2 \times 10^{11}$ cm; normalization is with respect to the peak of emission corresponding to the minor radius.

Similarly, for off-axis jet, the flux intensity and emission duration increase with radius; furthermore for given θ_{obs} and θ_{jet} the time at which the first photon is seen increases with R as shown in fig. 3.2

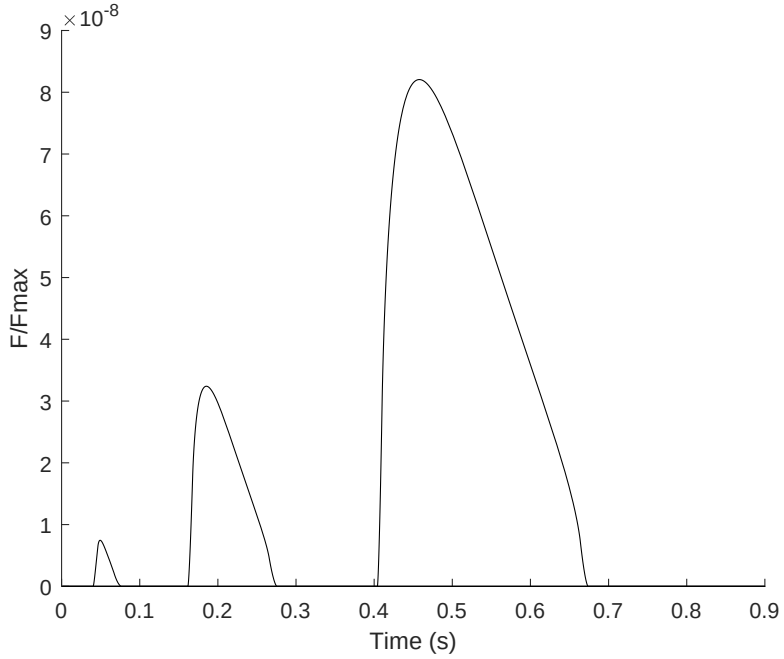

Fig. 3.2: Off-axis emission for $R = 2 \times 10^{10} - 8 \times 10^{10} - 2 \times 10^{11}$ cm, $T = 0.1$, $\theta_{obs} = 0.4$, $\theta_{jet} = 0.05$, $\Gamma = 30$; with the same normalization as fig. 3.1.

3.2 Dependence on T

The parameter T represents how long the surface of the sphere, or the jet, emits radiation: if

$$T \geq \frac{r(1-\cos(\theta_{obs}-\theta_{jet}))}{c} \tag{3.5}$$

it means that at a certain time the observer will see the whole surface emitting, leading to a saturation in the flux; otherwise, only a smaller portion at time is visible, then the flux will not reach the maximum. This is shown in fig. 3.3, an for on axis ($\theta_{obs} = 0$) jet with a given θ_{jet}.

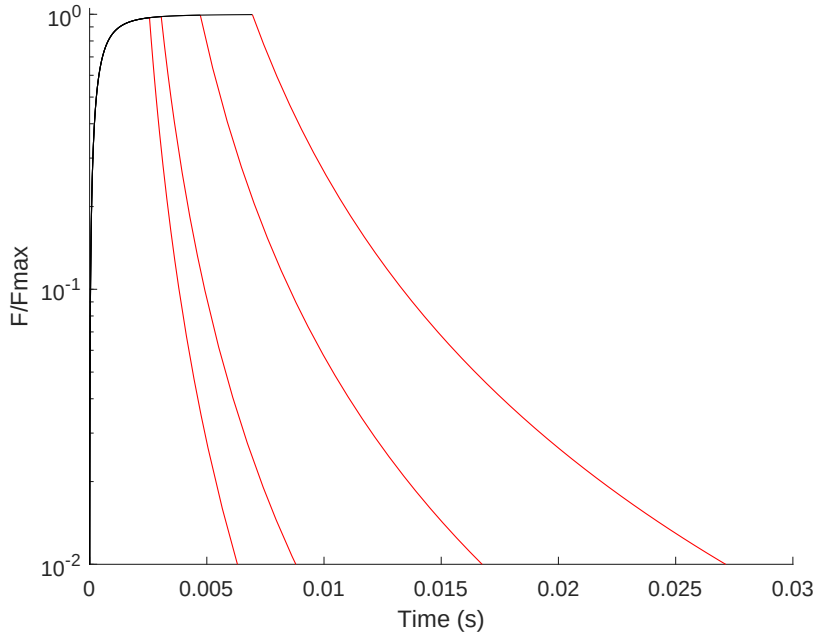

Fig. 3.3: Normalized flux for on axis jet for different values of $T = (0.2-1-2-4)$. In black the rising part of the light curve, that is the same for all T, in red the decaying part which depends on T.

The dependence on T of the off axis emission is quite similar to the on axis case: there is an increase in flux intensity for greater T, until saturation is reached, and also the duration of the signal is directly proportional to T.
The flux saturation value can be altered at later time by dynamical effects such as deceleration of the jet, sideways expansion and dependence on time of the specific intensity.

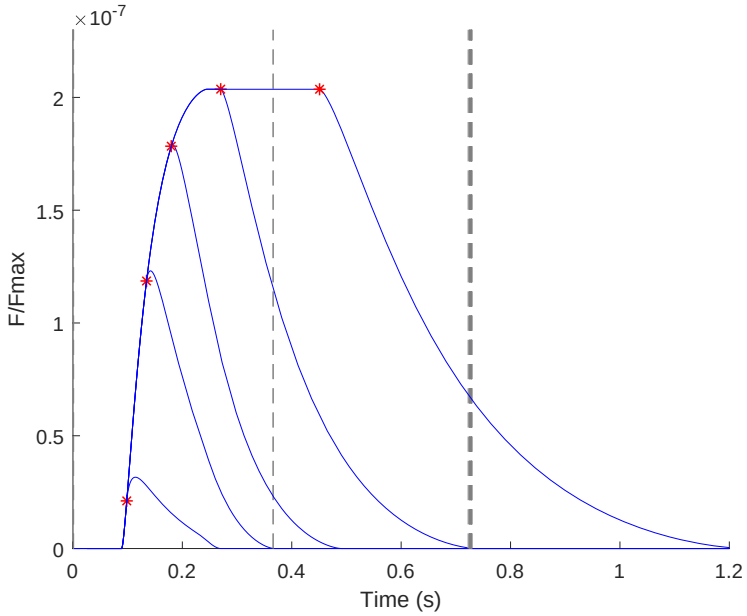

Fig. 3.4: Off axis light curves for T=(0.2-1-2-4-8) and $\Gamma = 30$, $\theta_{jet} = 0.1$, $\theta_{obs} = 0.4$, $R = 6 \cdot 10^{10}$ cm. There is a evident loss in precision for the time $t_{peak,off}$ (∗) for T=0.2-1.

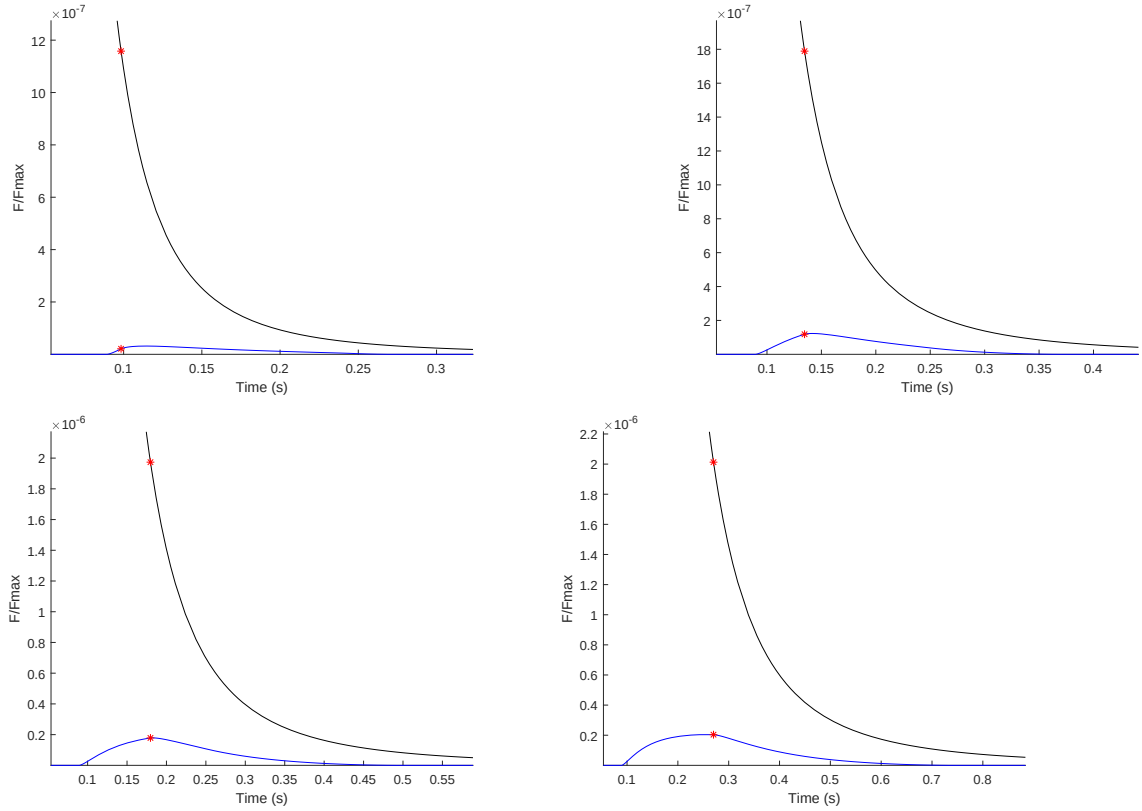

Fig. 3.5: Comparison between the on-axis light curve (-) and the off-axis one (-), both normalized to the maximum value of the on axis flux, with $T = (0.2 - 1 - 2 - 4)$ s (clockwise from top left) and $\Gamma = 30$, $\theta_{jet} = 0.1$, $\theta_{obs} = 0.4$, $R = 6 \cdot 10^{10}$ cm. The values of the light curves at the peak time are highlighted with ∗.

3.3 Dependence on Γ

For the an on axis emission results that the time at which the peak occurs and the duration decrease with the increase of Γ, while the intensity increases, as shown in fig 3.6. This, together with the fact that since the radiation is emitted by a source moving with Γ, it is highly blue-shifted, could be the motivation to the shortness-hardness relation observed in most GRBs.
On the contrary, because the relativistic beaming limits the emission in a solid angle $\sim \Gamma^{-1}$ and for an off axis observer with $\theta_{obs} > \theta_j + 1/\Gamma$ the increase of the Lorentz factor lowers the observed flux .

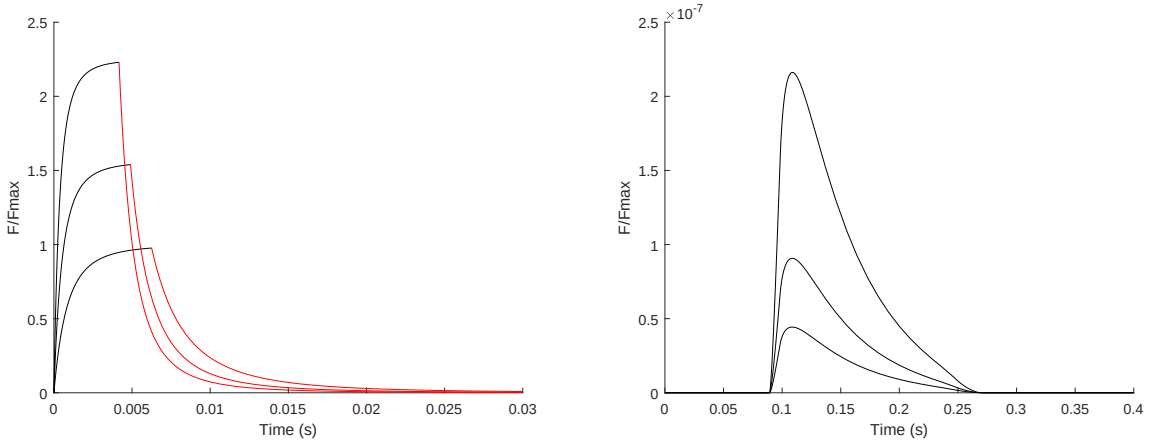

Fig. 3.6: Left: flux of an on axis uniform jet for $\Gamma = 20 - 25 - 30$ (from bottom to top), normalized with respect to the peak corresponding to $\Gamma = 20$. Right: light curves for off axis emission with $\Gamma = 20 - 25 - 30$ (from top to bottom) with the same normalization as left panel.

3.4 Dependence on θ_j

The jet opening is directly related to the observed flux because the emitting area is directly proportional to θ_j for both on and off axis jets and a larger area means a greater emission.
For on axis jets the effect of θ_{jet} is only to set the time at which the emission starts to decrease ($t_{peak,on}$), while the part of the light curve rising with time is totally unaffected.

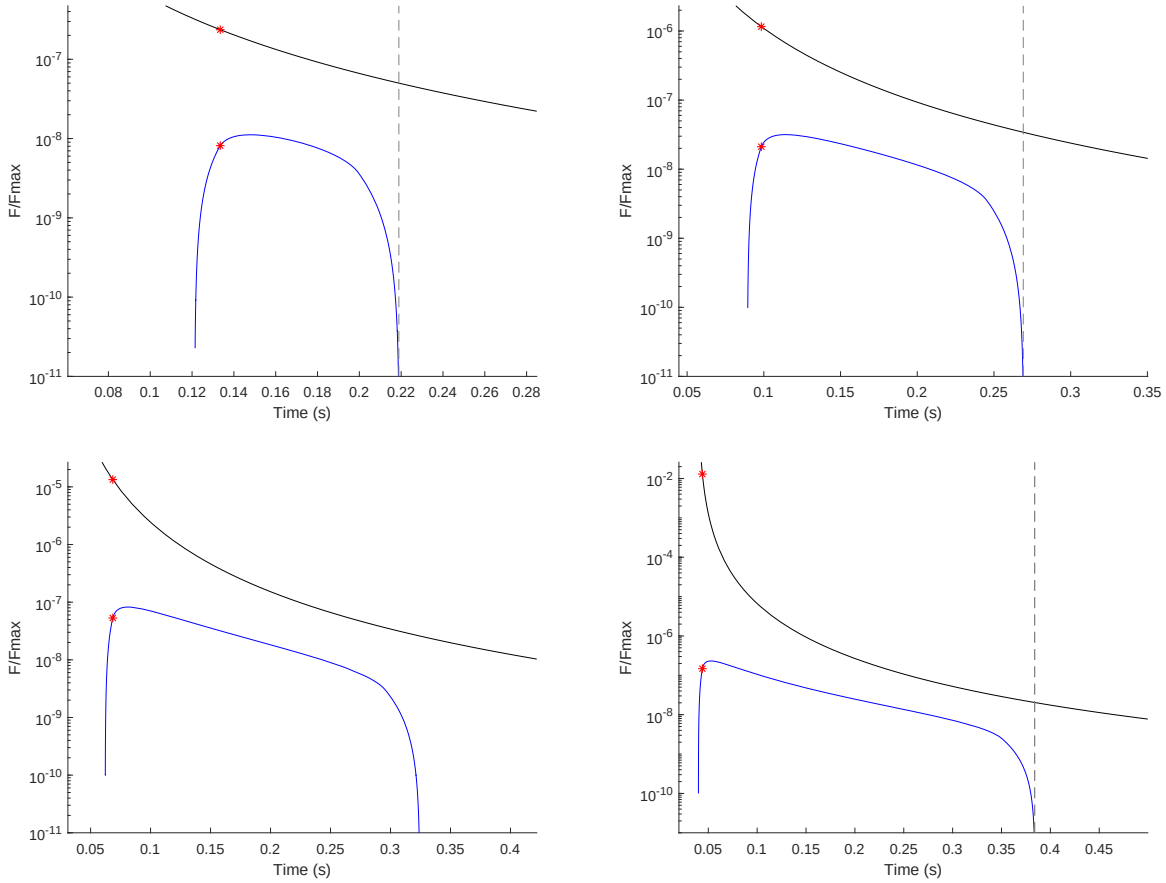

Fig. 3.7: Comparison between the on-axis light curve (-) and the off-axis one (-), both normalized to the maximum value of the on axis flux, with $\theta_j = (0.05 - 0.1 - 0.15 - 0.2)$ (clockwise from top left) and $\Gamma = 30$, $T = 0.2$ s, $\theta_{obs} = 0.4$, $R = 6 \cdot 10^{10}$ cm. The values of the light curves at the peak time are highlighted with $*$.

In the off axis case, things are a little different: the relation between opening angle and flux is the same as the on axis one, but also the time at which the emission is first seen depends on θ_j. In fact the photons emitted from the edge of the jet closer to the observer has to travel longer than the ones emitted from the tip of the sphere, producing a delay given by eqn. 3.2. Furthermore, since the photon emitted from the further edge on the jet has to travel even longer and that its distance from the observer increases with θ_j, the duration of the signal is directly proportional to the opening angle of the jet.

3.5 Dependence on θ_{obs}

The main effect of the angle of view is to decrease the intensity of the observed emission, as noticeable in fig. 3.8 representing the steep fall of the off axis flux peak corresponds to the increase of θ_{obs}. This happens because the relativistic beaming limits the most of the radiation in a cone of aperture $\sim \Gamma^{-1}$, the outside of it the emission is much dimmer.
An other effect of the increase of θ_{obs}, reported in fig. 3.9, is the delay of the time at which the first and also the last photons are seen, thus increasing the duration of the signal.

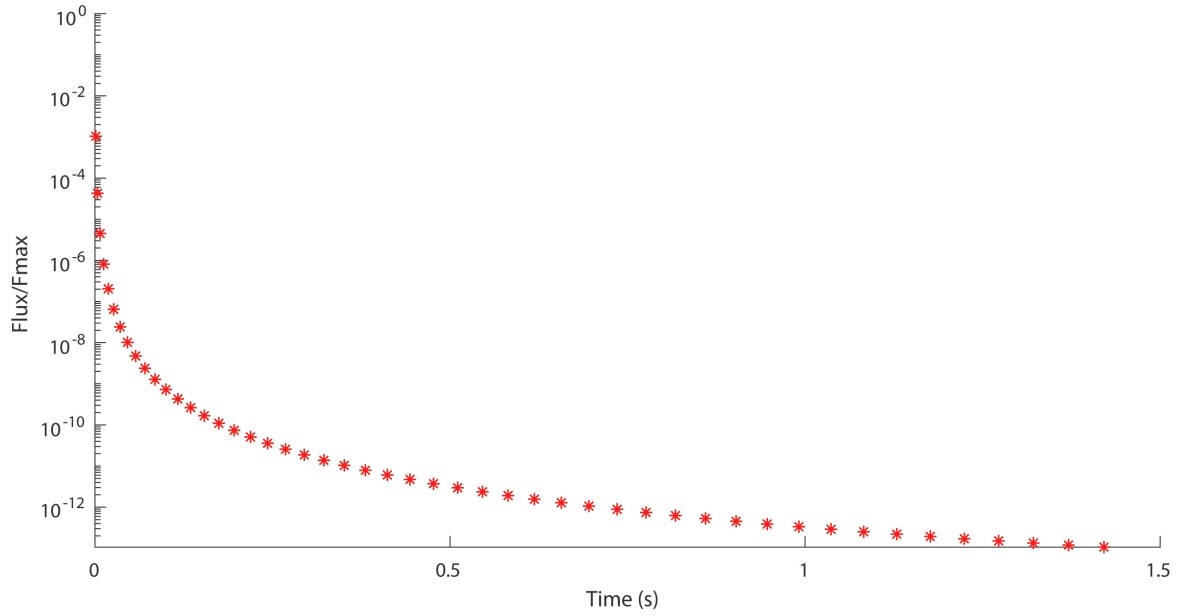

Fig. 3.8: Behaviour of the flux emission normalized peak for different angles of view, $\Gamma = 50$ $\theta_j = 0.01$, $T = 1$, $R = 6 \times 10^{10}$ cm.

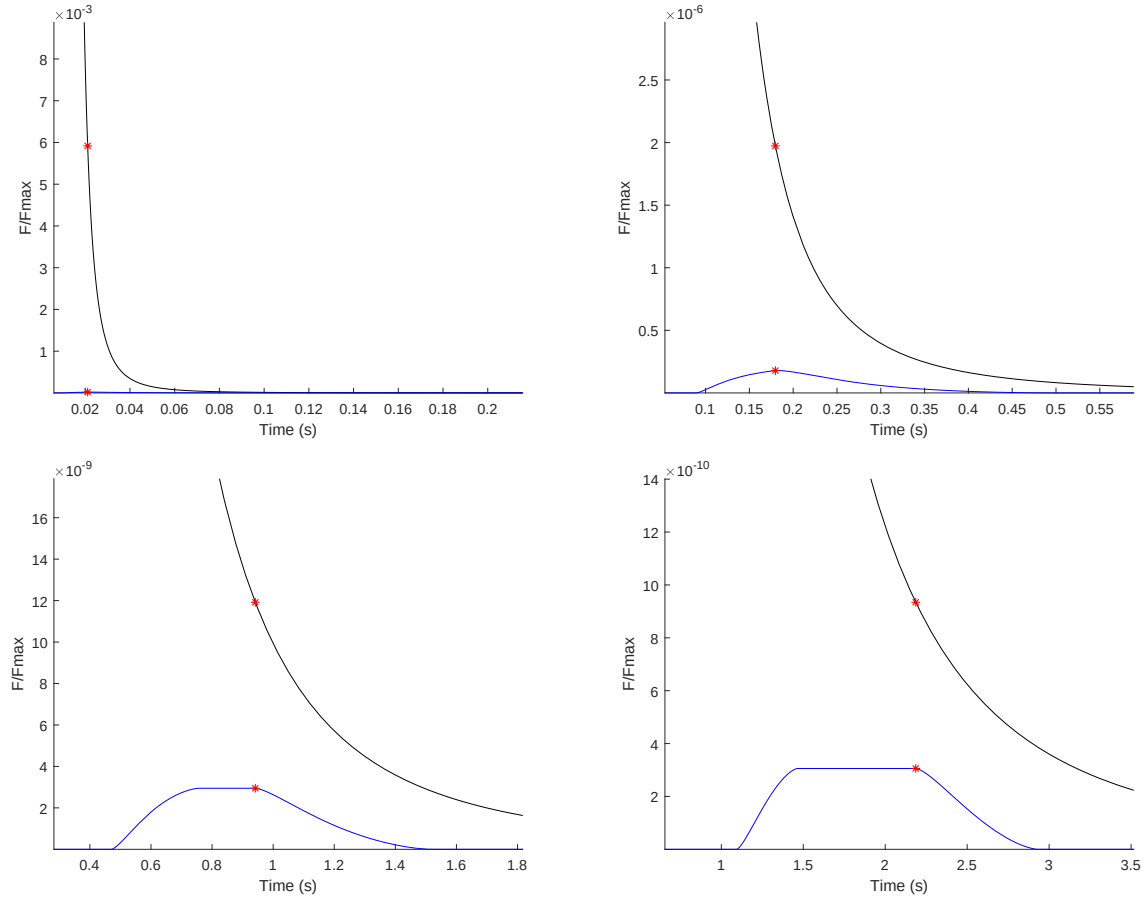

Fig. 3.9: Comparison between the on-axis light curve (-) and the off-axis one (-), both normalized to the maximum value of the on axis flux, with $\theta_{obs} = (0.2 - 0.4 - 0.8 - 1.2)$ (clockwise from top left) and $\Gamma = 30$, $T = 2$ s, $\theta_{jet} = 0.1$ $r = 6 \cdot 10^{10}$ cm. The values of the light curves at the peak time are highlighted with $*$. For the top left panel the value of the off-axis peak flux is $\sim 10^{-5}$.

4. SECOND ORDER MODEL

4.1 Temporal dependence of the Lorentz factor

As the ejected material travels further, it increases in mass collecting interstellar medium and, in the absence of continuous injection of energy from the central engine to the jet, it slows down. From Rohads 1999 and Sari, Piran and Halpern 1999 for an interstellar medium with density described by a power-law $\rho = n_0 r^{-s}$:

$$\Gamma(t) = \Gamma_0 (t/t_{jet})^{-3/8} \qquad for\ \ s = 0 \tag{4.1}$$

$$\Gamma(t) = \Gamma_0 (t/t_{jet})^{-1/4} \qquad for\ \ s = 2 \tag{4.2}$$

where

$$t_{jet} = 6.2(1+z)(E_{52}/n_0)^{1/3}(\theta_j/0.1)^{8/3}\ \text{hrs} \tag{4.3}$$

is the time at which the opposite edges of the jet enters in causal contact and E_{52} stands for $E/(10^{52}\ \text{erg})$. Hydrodynamic simulations lead to more accurate results, but generally still agree with this qualitative model.
Since temporal dependence can be introduced simply substituting $\Gamma \to \Gamma(t)$, its effects are straightforward to quantify because it is possible to extract the time dependence of the Lorentz factor from the integral of eqn. 2.55 since integration is with respect to θ and only through the extrema of integration the time dependence is introduced in the geometric model.
With regard to the prompt emission, there is not enough time to allow the Lorentz factor to vary much, thus time dependence of Γ can be neglected with a good approximation. Whereas, at later times when the jet has swiped a mass of interstellar medium comparable with its own, the decrease of its velocity has to be considered, because lower Γ means less beaming and so higher flux, but also softer radiation.

4.2 Sideways expansion

Sideways expansion of the jet effects the direction of motion of the ejected material and not only the jet aperture. It is still not clear what is the real behaviour of the expansion that in general depends on the density of the surrounding environment and on the characteristics (aperture, energy, density) of the jet.
Numerical simulations showed that sideways expansion does not have great effect on the prompt emission, on which I focused, because due to the briefness of the emission the jet has not enough time to expand and sideways expansion becomes important around t_j (Sari, Piran and Halpern 1999). Instead, at much later time, i.e. during the afterglow, the expansion is no more negligible, but since the velocity is already decreased to quasi- or sub-relativistic regime the beaming of the

emission becomes negligible and it is a good approximation to consider that the ejected material expanding spherically.

4.3 Structured jet

The previous sections were developed under the assumption of uniform jet: each point of the jet has the same velocity (represented by Γ), the same density (n) and then the same energy. More realistically the ejected material is more dense and fast in the inner region of the jet and at greater distance from the jet axis both n and Γ decrease due to the interaction with the surrounding medium. Their actual behaviours are not certain, the most probable are Gaussian and power law distributions; I chose the following expressions to describe density and velocity:

$$\Gamma(\theta) = \Gamma_{min} + (\Gamma_{max} - \Gamma_{min}) \left[1 - \frac{(\theta - \theta_{obs})^2}{k_1 \, \theta_{jet}^3} \right] \tag{4.4}$$

$$n(\theta) = n_{min} + 4 \, n_{max} \left[1 - \frac{(\theta - \theta_{obs})^2}{k_2 \, \theta_{jet}^3} \right] \tag{4.5}$$

where k_1 and k_2 are adimensional parameters used to adjust the slope of the distribution, I introduced the factor 4 in eqn. 4.5 to mimic the effect of an adiabatic shock on the density for a fluid moving with Lorentz factor Γ: $n_{shocked} \approx 4\Gamma n$ (Piran 2005, van Eerten et al. 2010).
Computing the light curve of a structured jet is a time requesting task, so an approximation was necessary: I divided the structured jet in uniform concentric sub-jets with half-opening decreasing by a constant factor $\Delta\theta$ and Lorentz factor and density given by evaluating eqn. 4.4 and 4.5 at $\theta = \theta_{jet} - \Delta\theta/2$. For each sub-jet eqn. 2.55 is evaluated and the resulting fluxes are summed, but doing this way there is an overcount of the area of the inner jets, so it is necessary to subtract eqn. 2.55 evaluated for the inner jet half-opening and the outer one Lorentz factor. This is done in the hypothesis of infinitesimally thin shell, otherwise the model presented is no longer a good approximation because the shape of the equal arrival time surfaces depends on the actual shape of the jet.

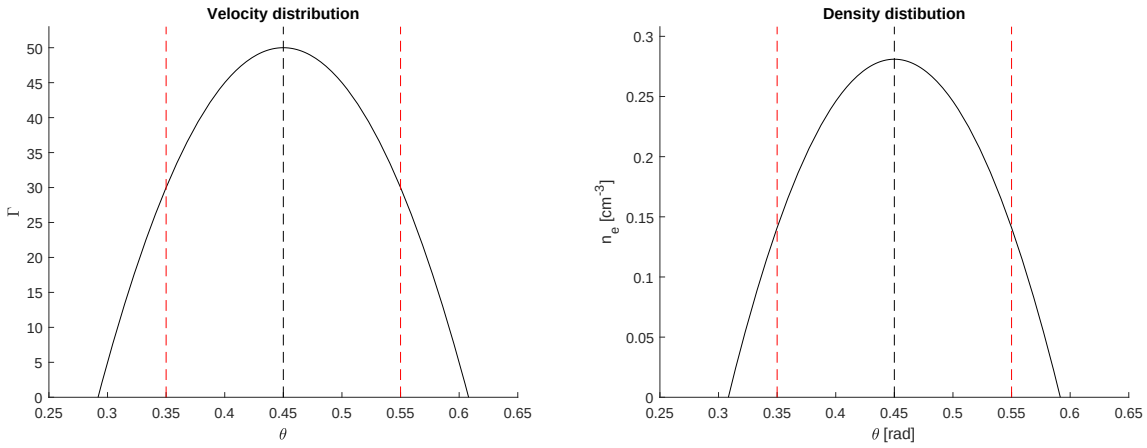

Fig. 4.1: Shape of the Γ (left) and density (right) distributions.

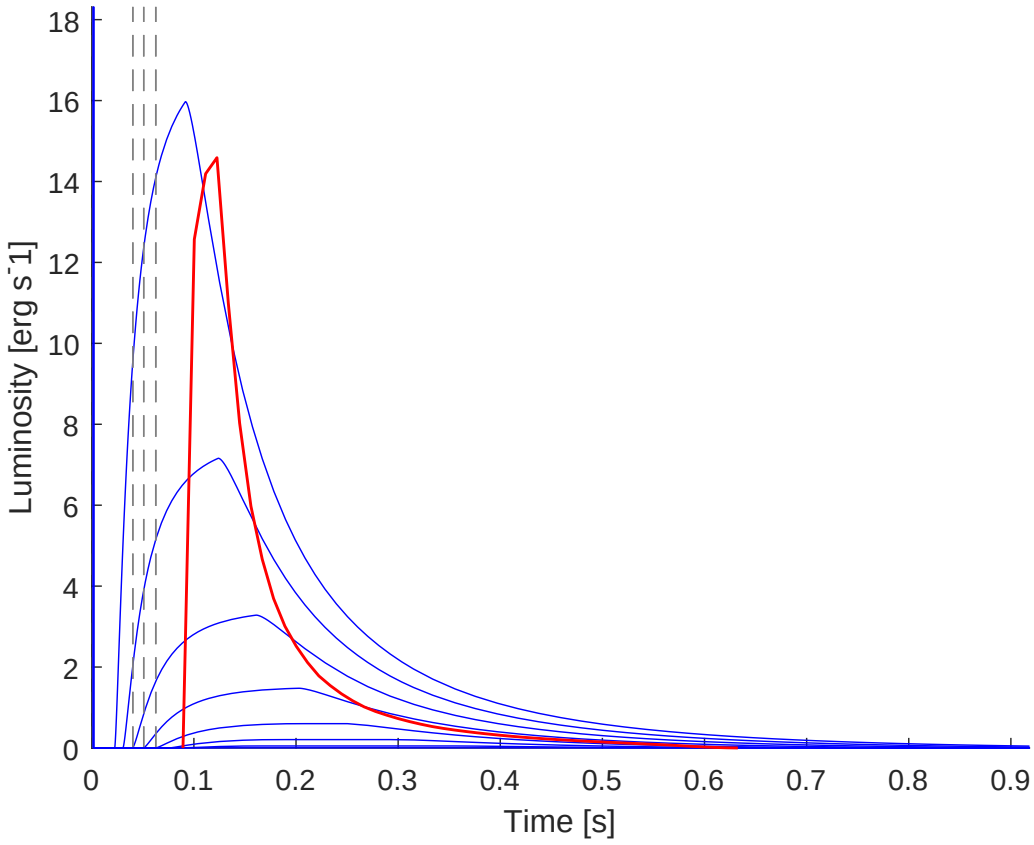

Fig. 4.2: Light curve for an off axis structured jet (-) with distribution of Γ 4.4 and density 4.5, compared to the ones from the single sub-jets. The luminosity scale is arbitrary.

5. COMPARISON WITH THE LITERATURE

The hypothesis regarding origin and mechanism of GRBs are many and different; the lack of an analytical model exactly fitting all the different aspects, from the dynamics of the ejected material to the emission process, makes numerical simulation the most viable way to obtain realistic results. However also from the most simple and idealized models is possible to obtain a qualitative behaviour representing the variation of observed flux in function of the angle between the line of sight and the jet.
For example Lazzati et al. (2017) proposed a model for sGRBs from binary mergers in which initially a collimated jet is ejected, then propagating in a dense and baryon rich environment, it produce a hot, wide cocoon which is responsible for the prompt emission. First, they considered a central engine releasing E_2 energy for a period of time t_{eng} in two opposite jets of half-opening θ_j which are accelerated up to a Lorentz factor Γ, giving a total isotropic equivalent energy $E_{iso} = 4\pi E_2/\Omega_2$ where Ω_2 is the solid angle occupied by the to jets. The prompt emission of the sGRB is computed considering top-hat uniform jet with sharp edges, radiating its internal energy at a certain distance R_{rad} from the centre of the engine. The nature of the emission is not discussed and considered irrelevant to the conclusions of the work.
The observed peak bolometric luminosity with respect to the observer angle is calculated as:

$$L_{prompt,pk}(\theta_{obs}) = L_{prompt,pk}(0)\frac{\int_\Sigma \delta^4(\Gamma,\theta_{v,obs})\, d\sigma}{\int_\Sigma \delta^4(\Gamma,\theta_v)\, d\sigma} \tag{5.1}$$

where $L_{prompt,pk}(0)$ is the peak bolometric luminosity for an on-axis observer, $\delta(\Gamma,\theta)$ is the relativistic Doppler factor, $\theta_{v,obs}$ is the angle between the velocity and the observer, θ_v is the angle between the velocity and the jet axis and the integral is performed over the emitting surface Σ. As soon as the line of sight moves outside the opening angle of the jet the peak luminosity of the prompt emission decreases dramatically as shown in fig. 5.1.
The model was developed further, through simulations, in order to account also the emission of the cocoon and the dynamical effects, but since the cocoon is expected to expand quasi-spherically and with decreasing Lorentz factor the emission will tend to become isotropic, thus the dependence on the observer angle ceases.

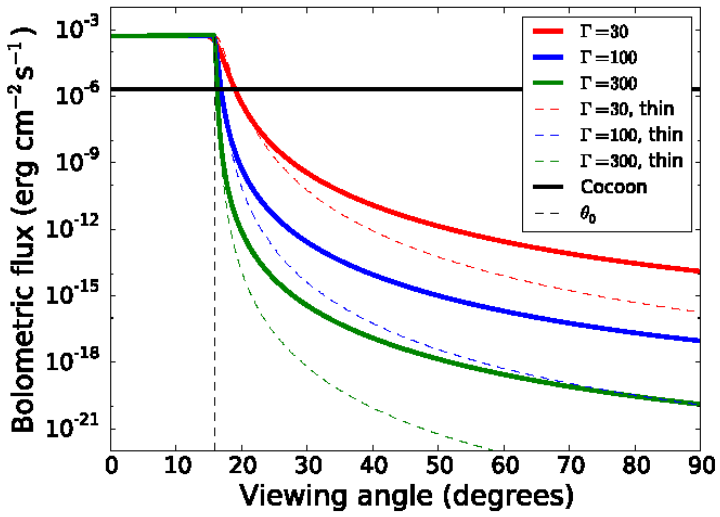

Figure 1. Bolometric peak flux of the prompt emission of a short GRB as a function of the observer viewing angle. The burst characteristics are from the fiducial values in Table 1 and are located at a distance of 200 Mpc from the Earth. Three values of the Lorentz factor are shown, as well as the isotropic cocoon contribution. The thin dashed line shows the result for a radially thin outflow that emits for a vanishingly small time.

Fig. 5.1: Figure 1 from Lazzati et al. 2017, to confront with fig. 5.2

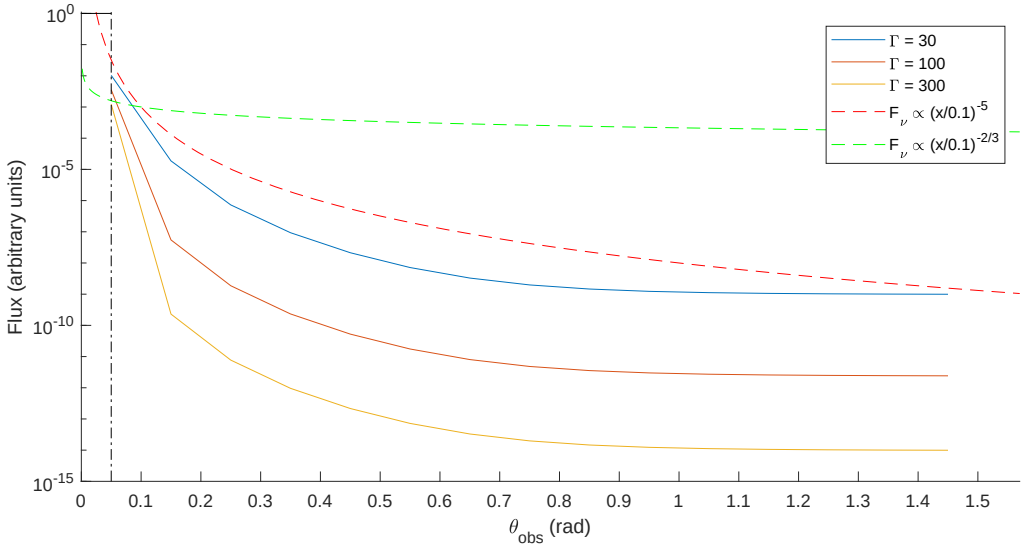

Fig. 5.2: Behaviour of the peak of the light curve, normalized with respect to the on axis peak, depending on θ_{obs} for different values of Γ. The vertical line represents the half-opening angle of the jet. The dashed lines are qualitative behaviours from Granot et al. 2002. It is evident the similarity in the decay of the intensity for increasing viewing angle with the ones reported in fig. 5.1.

A more sophisticated model is presented by Granot et al. 2002. The GRB emission for off-axis observer is calculated considering 3 different models of jet propagating in an homogeneous

medium: a point source moving along the jet axis, an homogeneous jet and a two-dimensional hydrodynamical simulation.
The first model has the advantage to be very simple, but it is limited to $\theta_{obs} > 2\theta_{jet}$ ant $t > t_{jet}$ with

$$t_{jet} = 6.2(1+z)\left(\frac{E_{52}}{n}\right)^{1/3}\left(\frac{\theta_{jet}}{0.1}\right)^{-8/3} \text{ hours} \tag{5.2}$$

The flux of a point source moving with Lorentz factor Γ at an angle θ with respect to the observer is given by:

$$F_\nu = \frac{1+z}{4\pi D_L^2}\frac{L'_{\nu'}}{\Gamma^3(1-\beta\cos\theta)^3} \tag{5.3}$$

where D_L is the luminosity distance, $L'_{\nu'}$ and ν' are the comoving spectral luminosity and frequency. Then, given t_0 and ν_0 the time and frequency for an on-axis observer, it results

$$\frac{\nu}{\nu_0} = \frac{t_0}{t} = \frac{1-\beta}{(1-\beta\cos\theta)} \equiv a \approx (1+\Gamma^2\theta^2)^{-1} \tag{5.4}$$

$$F_\nu(\theta_{obs},t) = a^3 F_{\nu/a}(0,at) \tag{5.5}$$

The second model is based on a jet with values of energy and Lorentz factor constant with respect to θ, but varying in time, with deceleration and sideways expansion determinated by the laws of mass and energy conservation as described in Kumar and Panaitescu 2000. The emission is due to both synchrotron and inverse Compton and the flux is calculated integrating over equal arrival time surfaces.
The two-dimensional hydrodynamical simulation is described in Granot et al 2001; it is more realistic and considers jets with smoother edges.
They obtained a qualitative behaviour from the first model describing the time and intensity at the luminosity peak:

$$t_{peak} \approx (5+2\ln\Theta)\Theta^2 t_{jet} \tag{5.6}$$

$$L_{peak} \approx 2^{-\beta+3}\Theta^{-2\alpha}L(0,t_{jet}) \tag{5.7}$$

where $\Theta = (\theta_{obs}/\theta_{jet}) - 1$, $\alpha \sim 2$ and $\beta \sim 1$ are parameters describing the dependence of L on time $L \propto t^{-\alpha}$ and frequency $L \propto \nu^{-\beta}$. As shown in fig. 5.3, this simple model overestimates the intensity of the light curve with respect to the other more complex ones, but describes quite well the overall behaviour specially at grater times and observer angles. Comparing the second model with respect to the simulation, the light curve produced by the homogeneous jet overestimates at almost all times and angle the one derived from the more complex, however for $\theta_{obs} < \theta_{jet}$ the results are quite similar. It is noticeable that light curves obtained from the simulations are more intense at early time, because the emission from the outer, slower region of the jet, neglected in the case of a hard edged homogeneous one, dominates.

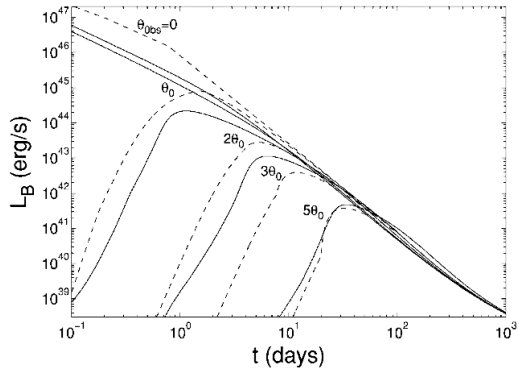

FIG. 1.—B-band luminosity for models 1 (*dashed lines*) and 2 (*solid lines*) for $\theta_0 = 5°$, $\theta_{obs} = (0, 1, 2, 3, 5)\theta_0$, $E_{52} = 80$, $n_0 = 1$, $p = 2.5$, $\epsilon_B = 0.01$, and $\epsilon_e = 0.1$, where ϵ_B and ϵ_e are the fraction of the internal energy in the magnetic field and electrons, respectively, and p is the power-law index of the electron energy distribution. Note that model 1 is scaled down by a factor of 2.5 to help compare between the two models.

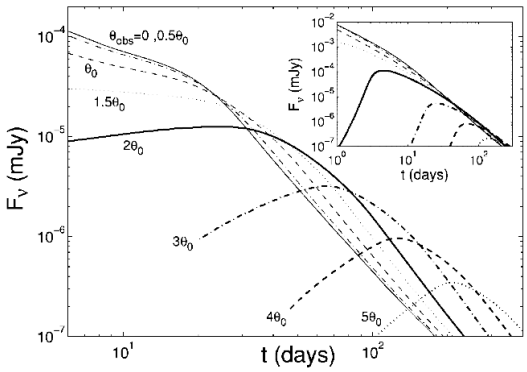

FIG. 2.—Light curves of model 3 for $\theta_0 = 0.2$, $E_{52} = n_0 = z = 1$, $p = 2.5$, $\epsilon_e = 0.1$, $\epsilon_B = 0.01$, and $\nu = 5 \times 10^{14}$ Hz. The inset shows the same light curves for model 2, where the same traces correspond to the same viewing angles θ_{obs}.

Fig. 5.3: Figure 1 and 2 from Granot et al. 2002. Even if the scales are different the similarity with fig. 4.2 is evident.

In J.Granot et al. 2018, it is presented a simple analytic model for off-axis emission from GRB jets showing the dependence of the observed flux on the angle of view θ_{obs} and many other parameters related to the ejecta. The starting point is the assumption that the jet of opening angle θ_j propagates as if it was spherical as long as $\Gamma > \theta_j^{-1}$, with equivalent isotropic energy

$$E_{iso} = \frac{E}{1-\cos\theta_j} \approx \frac{2\,E}{\theta_j^2} \tag{5.8}$$

$$E = \frac{2\pi}{3}\theta_j^2 R^3 \Gamma^2 n\, m_p c^2 \tag{5.9}$$

where n is the ambient density and m_p the mass of the proton. Sideways expansion starts when $\Gamma \sim \theta_j^{-1}$, thus the spherical phase ends and results

$$E = \frac{2\pi}{3} R^3 n\, m_p c^2 \tag{5.10}$$

The observer time is given by

$$t = (1+z)\frac{R}{4c\Gamma^2} \tag{5.11}$$

thus the jet break time can be expressed as (see also Sari, Piran and Halpern 1999)

$$t_b = 0.7(1+z)\left(\frac{E_{51}}{n}\right)^{1/3}\left(\frac{\theta_j}{0.1}\right)^2 \text{ days} \tag{5.12}$$

the notation $E_{51} = E/10^{51}$ is used. Because of the relativistic beaming the off-axis observer will see the afterglow only near its peak at $t_{peak}(\theta_{obs})$ given by:

$$t_{peak}(\theta_{obs}) = A\left(\frac{\theta_{obs}}{\theta_j}\right)^2 t_j = 70(1+z)\left(\frac{E_{51}}{n}\right)^{1/3}\theta_{obs}^2 \quad \text{days} \tag{5.13}$$

where $A \sim 1$, the flux rises until t_{peak} and then decays as for an on-axis observer.
From the universal post jet break light curve for an on-axis observer obtained by Nakar, Piran, Granot 2002, normalized to the optical frequency 5×10^{14} Hz; the peak of the flux above self absorption frequency is given by:

$$\begin{aligned} F^{peak}_{\nu>\nu_m,\nu_c}(\theta_{obs}) =& 1.67\frac{g_0(p)}{g_0(2.2)}A^{-p}(1+z)^{(1-p)/2}D_{L,28}^{-2}(1+Y)^{-1} \\ & \times \varepsilon_{e,-1}^{p-1}\varepsilon_{B,-2}^{(p-2)/4}n^{(3p-2)/12}E_{50.7}^{2/3}\nu_{14.7}^{-p/2}\theta_{obs,-1}^{-2p} \quad \text{mJy} \end{aligned} \tag{5.14}$$

$$\begin{aligned} F^{peak}_{\nu_m<\nu<\nu_c}(\theta_{obs}) =& 0.618\frac{g_1(p)}{g_1(2.2)}A^{-p}(1+z)^{(3-p)/2}D_{L,28}^{-2} \\ & \times \varepsilon_{e,-1}^{p-1}\varepsilon_{B,-2}^{(p+1)/4}n^{(p+1)/4}E_{50.7}\nu_{14.7}^{(1-p)/2}\theta_{obs,-1}^{-2p} \quad \text{mJy} \end{aligned} \tag{5.15}$$

$$\begin{aligned} F^{peak}_{\nu_a<\nu<\nu_m<\nu_c}(\theta_{obs}) =& 4.4\frac{g_2(p)}{g_2(2.2)}A^{-1/3}(1+z)^{4/3}D_{L,28}^{-2} \\ & \varepsilon_{e,-1}^{-2/3}\varepsilon_{B,-2}^{1/3}n^{1/3}E_{50.7}\nu_{9.93}^{1/3}\theta_{obs,-1}^{-2/3} \quad \text{mJy} \end{aligned} \tag{5.16}$$

where z is the cosmological red-shift, Y the Compton parameter D_L the luminosity distance, g_0, g_1 and g_2 are functions depending only on the index p,ε_e and ε_B are adimensional parameters representing the fraction of internal energy belonging respectively to the electrons and the magnetic field, ν_m is the frequency of maximum synchrotron emission, ν_c the cooling one and ν_a the self-absorption one given by

$$\begin{aligned} \nu_c =& 3.62\times 10^{15}\left[\frac{2.16}{1.22}\frac{(p-0.98)}{(p-0.04)}\right]^2 10^{\frac{2.2-p}{1.985}}(1+z)^{-1} \\ & \times \varepsilon_{B,-2}^{-3/2}n^{-5/6}E_{50.7}^{-2/3}(1+Y)^{-2} \quad \text{Hz} \end{aligned} \tag{5.17}$$

$$\begin{aligned} \nu_m =& 3.74\times 10^{11}\left[\frac{g_1(p)g_2(2.2)}{g_1(2.2)g_2(p)}10^{\frac{2.2-p}{3.93}}\right]^{\frac{6}{3p-1}}(1+z) \\ & \times \varepsilon_{B,-2}^{1/2}\varepsilon_{e,-1}^{2}n^{-1/6}E_{50.7}^{-2/3}t_{\text{days}}^{-2} \quad \text{Hz} \end{aligned} \tag{5.18}$$

It has to be stressed that the flux peak is independent of θ_j and strongly dependent on θ_{obs}. Indeed the chosen values for the parameters, derived from both long and short GRBs, are $\varepsilon_e = 0.1$, $\varepsilon_B = 0.01$, $p = 2.5$, $n = 1$, $8^\circ < \theta_j < 16^\circ$ and $E \sim 10^{48} - 10^{49}$ erg. Unfortunately, the dependence on Γ is hidden in the other parameters, namely ε_e, ε_B, n and E, which are related to the hypotheses on the shock characteristics through non trivial relations; thus the dependence of the flux peak on the observer angle:

$$F^{peak}_{\nu>\nu_m,\nu_c}(\theta_{obs}) \propto \left(\frac{\theta_{obs}}{0.1}\right)^{-5} \tag{5.19}$$

$$F^{peak}_{\nu_m<\nu<\nu_c}(\theta_{obs}) \propto \left(\frac{\theta_{obs}}{0.1}\right)^{-5} \tag{5.20}$$

$$F^{peak}_{\nu_a<\nu<\nu_m<\nu_c}(\theta_{obs}) \propto \left(\frac{\theta_{obs}}{0.1}\right)^{-2/3} \tag{5.21}$$

Since the expression from Granot et al. 2018 lack of explicit dependence on many parameters relevant to the proposed model what matters in the fig. 5.4 and 5.5 is that the curves are almost parallel, showing that the qualitative behaviour is similar.

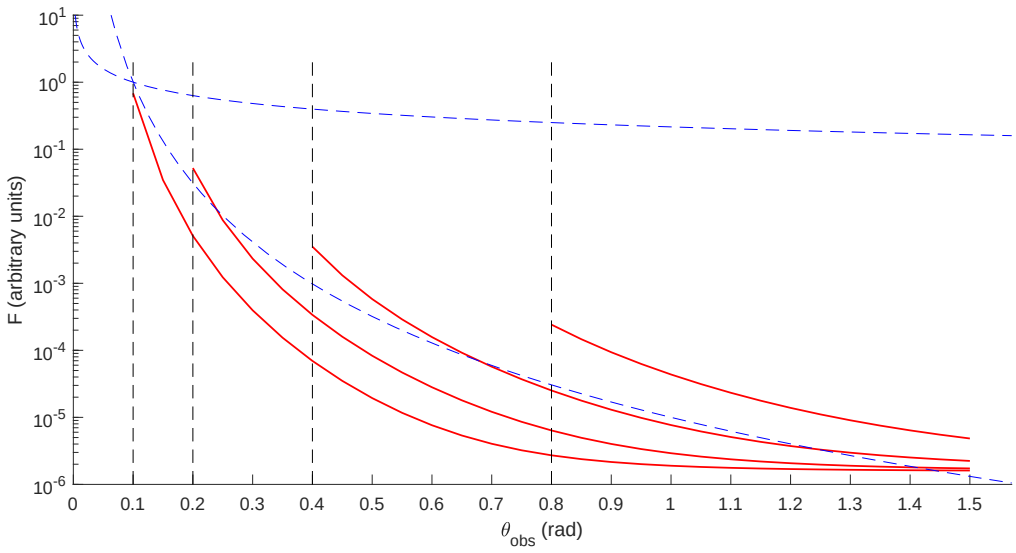

Fig. 5.4: Proposed model (-) for different values of $\theta_{jet} = 0.05 - 0.1 - 0.2 - 0.4$ (from left to right), eqn. 5.20(– bottom) and eqn. 5.21(– top).

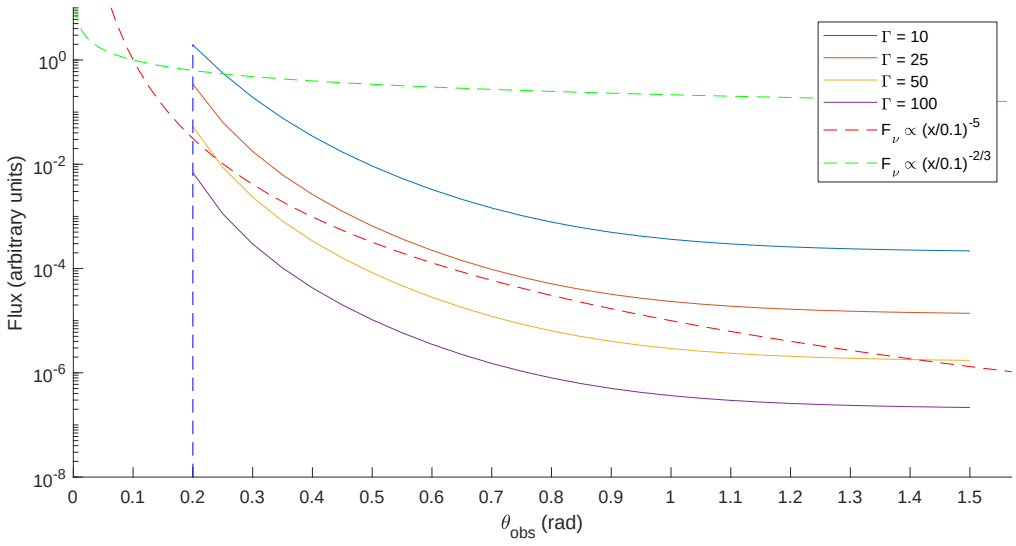

Fig. 5.5: Proposed model (line in different colours) for different values Γ, eqn. 5.20(– bottom) and eqn. 5.21(– top).

However, numerical simulations have shown that the simply analytic model for a uniform jet is not correct. Instead a structured jet with a more energetic and faster central region and a less energetic and slower outer region whose expansion direction is not exactly radial, but points more sideways is more realistic. The outer region dominates the early emission for large viewing angles, since it has lower Γ and thus the emission is spread on a wider solid angle with respect to the one generated by the central region. Indeed the analytic peak flux prediction is higher than that of the numerical simulation by around an order of magnitude and for certain values of t the discrepancy is even higher.
From the gravitational waves data of GW170817, supposing that the jet is aligned with the total orbital momentum of the binary system, the values of $\theta_{obs} = 0.6 \pm 0.1$ are assumed. Furthermore the unusually low isotropic equivalent energy in the γ-ray region measured of $E_{\gamma,iso} = (5.36 \pm 0.38) \times 10^{46}\ D^2_{40\,\mathrm{Mpc}}$ and the peak energy $\nu F_\nu = 40 - 185$ keV suggest that GRB170817A has been produced by a jet seen off-axis, composed of a roughly uniform core of half-opening θ_0 and in the surrounding region the energy per unit solid angle decays gradually. The resulting flux density is, for the different intervals of frequency:

$$F_{\nu>\nu_m,\nu_c}(t) = 1.18\frac{g_0(p)}{g_0(2.2)}10^{1.78(2.2-p)}D^{-2}_{40\,\mathrm{Mpc}}(1+Y)^{-1} \times \varepsilon_{e,-1}^{p-1}\varepsilon_{B,-2}^{(p-2)/4}E_{46.64}^{\frac{p+2}{4}}\nu_{14.7}^{-p/2}t_{days}^{\frac{2-3p}{4}} \quad \mu\mathrm{Jy} \tag{5.22}$$

$$F_{\nu_m<\nu<\nu_c}(t) = 0.0131\frac{g_1(p)}{g_1(2.2)}10^{1.78(2.2-p)}D^{-2}_{40\,\mathrm{Mpc}} \times \varepsilon_{e,-1}^{p-1}\varepsilon_{B,-2}^{(p+1)/4}E_{46.64}^{\frac{p+3}{4}}n^{1/2}\nu_{14.7}^{(1-p)/2}t_{days}^{\frac{3-3p}{4}} \quad \mu\mathrm{Jy} \tag{5.23}$$

$$F_{\nu_a<\nu<\nu_m<\nu_c}(t) = 0.196\frac{g_2(p)}{g_2(2.2)}D^{-2}_{40\,\mathrm{Mpc}} \times \varepsilon_{e,-1}^{-2/3}\varepsilon_{B,-2}^{1/3}n^{1/2}E_{46.64}^{5/6}\nu_{9.93}^{1/3}t_{days}^{1/2} \quad \mathrm{mJy} \tag{5.24}$$

substituting in the previous eqn. 5.13 an expression for the peak flux is obtained.
The values $\theta_0 = 0.2$, $n = 1$ and $E_{iso} = 10^{53}$ erg were used as first approximation to start the fit of the numerical model with the measurements in X-ray and radio, which gave as result: $E \sim (10^{48.5} - 10^{49.5})\xi_{e,-1}^{-1}$ erg, circumburst density $n \sim (10^{-5} - 10^{-2})\xi_{e,-1}^{-1}$ cm^{-3} for viewing angle $\theta_{obs} \sim 0.28 - 0.45$, $\varepsilon_e \sim (10^{-1.7} - 10^{-0.7})\xi_{e,-1}$, $\varepsilon_B \sim (10^{-5.6} - 10^{-1.7})\xi_{e,-1}$, power law index for the energy distribution of the radiating electrons $p \approx 2.2$, where $\xi_e \sim 0.1$ is a parameter representing the non-thermal acceleration efficiency of the shock on the electrons.

An other simple model is presented by E. Rossi et al 2002.
First they considered a uniform jet with opening θ_j emitting synchrotron radiation and focused on the power law branch of the spectrum between ν_m and ν_c respectively the peak and cooling frequencies.
Given a frequency, an observer angle θ_o and a time t the observed flux is:

$$F(\nu,\theta_o,t) \propto A_e I'(\frac{\nu}{\delta},\delta t)\delta^3(\Gamma,\theta_o) \tag{5.25}$$

where A_e is the emitting area $\delta(\Gamma,\theta) = [\Gamma(1-\beta\cos\theta)]^{-1}$ is the relativistic Doppler factor. I' is the co-moving intensity at the co-moving frequency $\nu' = \nu/\delta$ at the co-moving time $t' = \delta\, t$;

$$I' = I'(\nu'_m, t')\left(\frac{\nu'}{\nu'_m}\right)^{-\alpha} \propto \Gamma^{2+3\alpha}\delta^{1+\alpha} t\ \nu^{-\alpha} \tag{5.26}$$

with α depending on the chosen frequency interval.
Due to the relativistic beaming the observed flux depends on the observer angle; in particular for the on axis case ($\theta_o \approx 0$)

$$F = F_{on} \approx \pi\left(\frac{R}{\Gamma}\right)^2 I'\ (2\Gamma)^3 \quad \forall t \tag{5.27}$$

while for the off-axis case ($\theta_o > \theta_j$)

$$F = F_{off} \approx \begin{cases} \pi(R\theta)^2 I' \left(\frac{1}{\Gamma(1-\beta\cos\theta_o)}\right)^3 & t < t_b \\ \pi\left(\frac{R}{\Gamma}\right)^2 I'\ (2\Gamma)^3 & t > t_b \end{cases} \tag{5.28}$$

where t_b is the jet break time at which lateral expansion takes place and it is given by

$$t_b \propto \begin{cases} \theta^{2/3}\varepsilon^{1/3}\theta_o^2 \propto \theta_o^2 & for\ \ \theta \ll \theta_o \\ \theta^{8/3}\varepsilon^{1/3} \propto \theta^2 & for\ \ \theta \gg \theta_o \end{cases} \tag{5.29}$$

where ε is the energy per unit solid angle, described by the power law

$$\varepsilon = \begin{cases} \varepsilon_c & for\ \ 0 \le \theta \le \theta_c \\ \varepsilon_c\left(\frac{\theta}{\theta_c}\right)^{-2} & for\ \ \theta_c \le \theta \le \theta_j \end{cases} \tag{5.30}$$

with θ_c introduced to avoid divergences in $\theta = 0$ limited to be greater than $\Gamma_{max}^{-1} \sim 10^{-3}$deg.
Also the Lorentz factor follows a power law:

$$\Gamma = \begin{cases} \Gamma_c & for\ \ 0 \le \theta \le \theta_c \\ \Gamma_c\left(\frac{\theta}{\theta_c}\right)^{-\alpha_\Gamma} & for\ \ \theta_c \le \theta \le \theta_j \end{cases} \tag{5.31}$$

with $\alpha_\Gamma > 0$, this index is not important to the dynamic and the computation of light curve as long as $\Gamma(t = 0, \theta) \equiv \Gamma_0(\theta) > \theta^{-1}$ and $\Gamma_0(\theta) \gg 1\ \forall\theta$.
The light curve from a inhomogeneous jet, with the characteristic described above, is computed dividing it in a number of concentric hollow cones, each one with energy and Lorentz factor given by eqns. 5.30 and 5.31 respectively, and summing the single light curves obtained considering the asymptotic behaviour related to the opening angle of the sub-cones.
The results are summarised in the following fig. 5.6

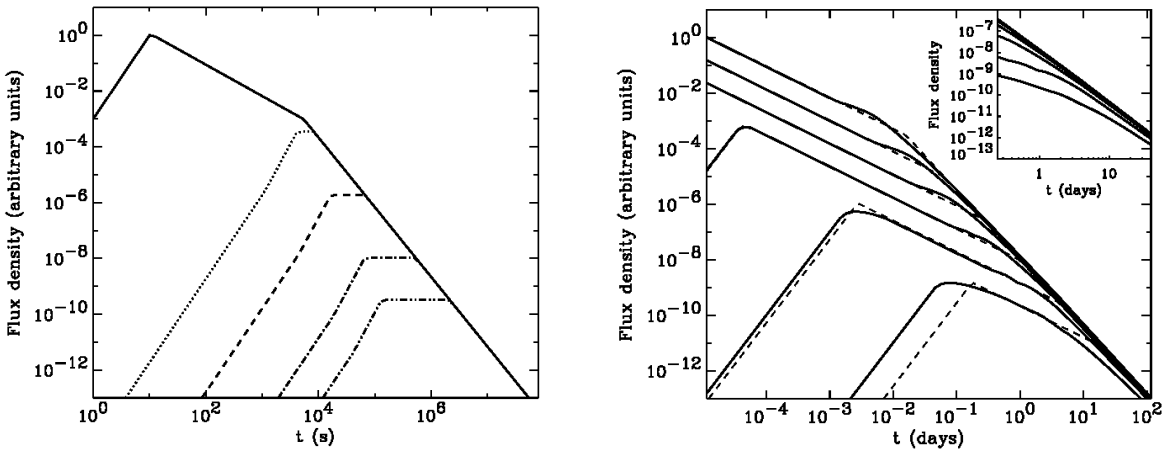

Fig. 5.6: Results from Rossi et al. 2002. Left panel: light curves of an homogeneous top-hat jet with opening $\theta_j = 1^\circ$ for angle of view $\theta_o = 0^\circ, 2^\circ, 4^\circ, 8^\circ$,from top to bottom. Right panel: light curves of an inhomogeneous jet with $\theta_j = 1^\circ$ and $\theta_o = 0.5^\circ, 1^\circ, 2^\circ, 4^\circ, 8^\circ, 16^\circ$; the dashed lines are the light curves for a top-hat homogeneous jet with opening angle $2\theta_o$ and energy per unit solid angle $\varepsilon(\theta_o)$.

Comparing fig. 5.6 and 4.2 it is noticeable that the qualitative behaviour is quite similar to the one obtained through the geometrical model represented by eqn. 2.55, for both top-hat homogeneous and structured jet. In the left panel of fig. 5.6 an horizontal part of the light curves is present, it happens because the whole surface is visible to the observer at the given angle and thus the flux reaches the maximum value, which lasts until the surface starts to turn off. This characteristic is present also in the proposed model and is mostly due to the geometry of the phenomenon rather than depending on the emission processes, as described in chapter 4.
A useful comparison between the models of jet with homogeneous characteristics, with Gaussian energy distribution and cocoon is reported in E. Troja et al. 2018. Through numerical simulation they compared the three models with the data regarding GRB170817A and obtained the best fit parameters reported in fig. 5.7.

Table 2. Constraints on the Gaussian jet and Cocoon model parameters. Reported are the median values of each parameter's posterior distribution with symmetric 68% uncertainties (ie. the 16% and 84% quantiles).

	Jet	Jet+GW+Planck	Jet+GW+SHoES
Parameter	Med.	Med.	Med.
θ_v	$0.51^{+0.20}_{-0.22}$	$0.32^{+0.13}_{-0.13}$	$0.43^{+0.13}_{-0.15}$
$\log_{10} E_0$	$52.50^{+1.6}_{-0.79}$	$52.73^{+1.30}_{-0.75}$	$52.52^{+1.4}_{-0.71}$
θ_c	$0.091^{+0.037}_{-0.040}$	$0.057^{+0.025}_{-0.023}$	$0.076^{+0.026}_{-0.027}$
θ_w	$0.55^{+0.65}_{-0.22}$	$0.62^{+0.65}_{-0.37}$	$0.53^{+0.70}_{-0.24}$
$\log_{10} n_0$	$-3.1^{+1.0}_{-1.4}$	$-3.8^{+1.0}_{-1.3}$	$-3.24^{+0.91}_{-1.3}$
p	$2.155^{+0.015}_{-0.014}$	$2.155^{+0.015}_{-0.014}$	$2.155^{+0.015}_{-0.014}$
$\log_{10} \epsilon_e$	$-1.22^{+0.45}_{-0.80}$	$-1.51^{+0.53}_{-0.89}$	$-1.31^{+0.46}_{-0.78}$
$\log_{10} \epsilon_B$	$-3.38^{+0.81}_{-0.45}$	$-3.20^{+0.92}_{-0.58}$	$-3.33^{+0.82}_{-0.49}$
$\log_{10} E_{tot}$	$50.26^{+1.7}_{-0.69}$	$50.16^{+1.1}_{-0.67}$	$50.19^{+1.41}_{-0.65}$

	Cocoon
Parameter	Med.
$\log_{10} u_{\max}$	$0.93^{+0.34}_{-0.36}$
$\log_{10} u_{\min}$	$-2.2^{+1.9}_{-1.9}$
$\log_{10} E_{\rm inj}$	$54.7^{+1.6}_{-2.7}$
k	$5.62^{+0.93}_{-1.1}$
$\log_{10} M_{\rm ej}$	$-7.6^{+2.1}_{-1.7}$
$\log_{10} n_0$	$-5.2^{+2.2}_{-2.0}$
p	$2.156^{+0.014}_{-0.014}$
$\log_{10} \epsilon_e$	$-1.33^{+0.93}_{-1.3}$
$\log_{10} \epsilon_B$	$-2.5^{+1.5}_{-1.1}$
$\log_{10} E^*_{tot}$	$52.84^{+0.97}_{-1.3}$

Fig. 5.7: Table 2 from Troja et al. 2018, reporting a summary of the values they obtained from the simulations.

They obtained that, as already seen, the early time emission is dominated by the slower external region of jets who do not have hard edges, as the Gaussian ones; while at later time the light curves are rather similar. Furthermore the early time emission from a uniform hard-edged jet seen off axis with $\theta_{obs} \sim 4\theta_{jet}$ is almost undistinguishable from the Gaussian jet one; at least until the first reaches the peak of intensity when, in the off axis case the intensity start decreasing leading to an underestimation of different order of magnitude.
All the three model produced results similarly consistent with data, due to the uncertainties on the environment and the many degeneracies in the parameters. The Gaussian and homogeneous models produce really similar results as shown in fig. 5.7 and lead to an angle of view of $0.32 - 0.43$ and 0.51 respectively. The cocoon interpretation leads to relatively slow ejecta $u \sim \Gamma \in [3.7;\ 18.6]$ with most of the energy in the slower material. However, the ejected mass and the minimum velocity of the distribution u_{min} are poorly constraint, leading to a uncertainty in the total energy which strongly depends on u_{min}. The main difference in these models is that the cocoon produces a higher total energy, $\sim 10^{52}$ erg while the others $\sim 10^{50}$ erg, and a less dense environment, $n_{cocoon} \sim 10^{-5.2}$ cm^{-3} while $n_{jet} \sim 10^{-3.8}$ cm^{-3}.
With regard to GRB170817A they obtained, from the best fit parameters of a Gaussian jet, a total isotropic equivalent energy in the γ-ray spectrum if seen on axis of $E_{\gamma,OA} \sim 2 \times 10^{51}$ erg, while the observed one is $E_{\gamma,obs} \sim 5 \times 10^{46}$ erg.

6. RESULTS

Through the relations 3.2-3.3 and the data on GRB170817A is possible to put more strict constraint on the characteristic of the phenomenon, but first is necessary to analyse in more detail the possibilities and make some hypothesis.
First of all the time delay between the detection of the gravitational waves peak and the prompt emission of γ-rays is kind of a mystery: there are different plausible reasons to it leading to different interpretation of the origin of the emission. The observed delay $\Delta t = 1.74 \pm 0.05$s is imputable to four main factors: the time necessary to the ejected material to fall back on the newborn object (t_{acc}); the delayed formation of a black hole; a delay in the emission itself; the jet has to travel up to a given radius in order to emit γ-rays (t_{prop}). However, the accretion time is really small: from B. B. Zhang et al. 2018

$$t_{acc} \sim 2\Big(\frac{2}{G\rho_{ns}}\Big)^{1/2} \sim 5 \cdot 10^{-4}\text{s} \tag{6.1}$$

thus it is negligible. Also the idea of a later black hole is to discard because the analysis of the extended gravitational emission (van Pullet, Della Valle 2018) shows that it is highly probable that the remnant of the merger and then the central engine of GRB170817A is a HMNS, since the gravitational signal detected 0.67s after the peak is compatible with the one emitted by an asymmetric spinning object, quite different from the one emitted during the ringdown of a black hole. The more plausible hypothesis is that the ejected material has to travel a certain distance in order to emit; in the case of synchrotron emission the time needed is reported by B.B.Zhang et al 2018 as:

$$t_{prop} \sim \frac{R}{\Gamma^2 c} \sim 1,74 \left(\frac{R}{5 \cdot 10^{14}\text{cm}}\right)\left(\frac{\Gamma}{100}\right)^{-2}\text{s} \tag{6.2}$$

that makes the most part of the delay, so

$$\Delta t = (1+z)\, t_{prop} \tag{6.3}$$

where $z \sim 0.009$ is the cosmological redshift for GRB170817A. Relation 6.2 is similar to eqn. 1.8 and thanks to both it is possible to reduce the degeneracy on the variables of the system: for a chosen Γ (or R) the appropriate R (or Γ) to obtain the observed delay is provided. For example from eqn. 1.8 given $\sigma_{decay} = 0.3$ and supposing $\Gamma = 50$ the resulting radius is 4.5×10^{13} cm and from eqn. 6.2 assuming the whole observed delay between GW and GRB is due to the propagation time, then $t_{prop} = t_{delay} - t_{10} = 1.42$ s and for the same Lorentz factor results $R \sim 10^{14}$ cm. Whereas if the inner engine required some time to start accelerating the jet and equating that time to the interval between the peak of gravitational waves and the signal associated with

a HMNS results: $t_{prop} = t_{delay} - t_{10} - t_{HMNS} = 0.75$ s giving $R \sim 5.6 \times 10^{13}$, really close to the one obtained from the eqn. 1.8 from Abbot et al 2017.
From the data of GRB170817 the peak of the light curve and thus the area is obtained; from the geometric model a synthetic light curve is produced for given values of R, Γ, θ_{jet}, θ_{obs} and T. In order to obtain the values of energy peak and fluence equivalent to the case of on axis jet it is necessary to find the values of the jet parameter that best fit the observed signal and then substituting them in the on axis model. Due to the complexity of eqn. 2.55 I was not able to perform a proper fit, whereas given the previous relations and the data obtained by others (see previous chapter) it is possible only to obtain a variety of plausible values for the parameters.

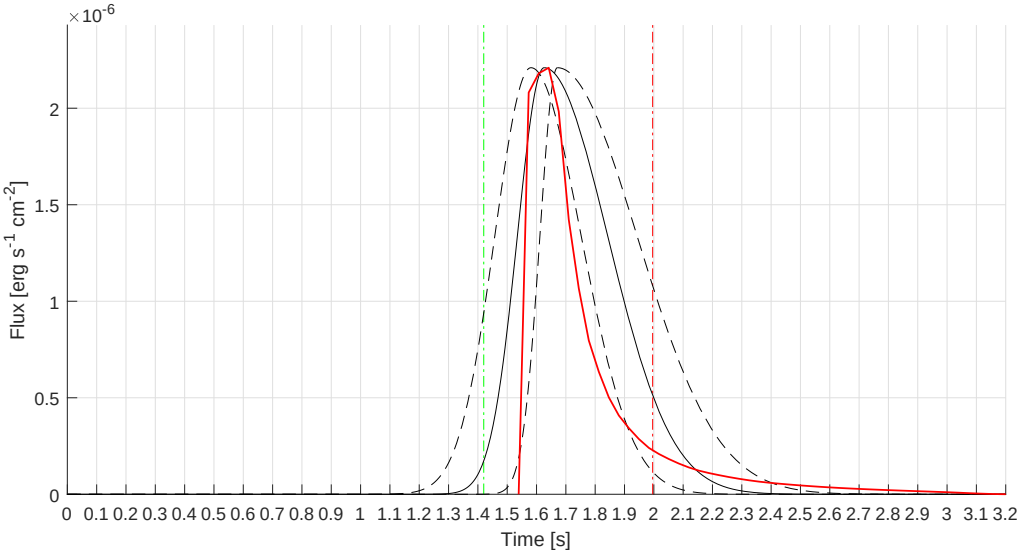

Fig. 6.1: Comparison between the proposed model (-) with $t_1 0$ (–), $t_9 0$ (–), the best fit curve (-) and relative errors (–) for the data of the first peak of GRB170817A (Goldstein 2017). The light curve is obtained from an off-axis structured jet with characteristics: $\theta_{jet} = 0.2$, $\theta_{obs} = 0.35$, $R = 10^{12}$ cm, $\Gamma_{min} = 10$, $\Gamma_{max} = 40$, $T = 20$, $n_{min} = 0.001$, $n_{max} = 0.009$, $B' = 10^{12}$ G.

Using the values of the parameters proposed by Granot et al. 2018, with the main aim to obtain a similar fluence value of $(1.4 \pm 0.3) \times 10^{-7}$ erg cm^{-2} (Abbot et al. 2017) and secondarily to fit the shape of the peak described by eqn. 1.5 and parameters 1.6, I chose the values $\theta_j = 0.2$, $\theta_{obs} = 0.35$, $R = 10^{12}$ cm, $\Gamma_{min} = 10$, $\Gamma_{max} = 40$, $T = 20$, $n_{min} = 0.001$, $n_{max} = 0.009$, $B' = 10^{12}$ G giving the light curve, translated by T0 - 0.32 s, reported in fig. 6.1. Unfortunately the light curve obtained from a structured jet with the given characteristics does not fit well the data of the first peak, but since their shape is approximatively the same (fast rise and slow decay), it does not seem unbelievable that the main behaviour is well described. Maybe the chosen distribution of velocity and density is not accurate and a flatter jet could produces a wider peak. I obtained a fluence of $(5.49 \pm 0.07) \times 10^{-7}$ erg cm^{-2}, a mean flux value of $(3.22 \pm 0.04) \times 10^{-7}$ erg s^{-1} cm^{-2}, resulting in a observed luminosity of $(4.9 \pm 0.3) \times 10^{45}$ erg s^{-1} if considered on axis. Otherwise, assuming the GRB170817A has been seen off-axis and considering the ratio between the peak flux value for both on and off axis light curves derived by the geometric model $F_{peak,ON}/F_{peak,OFF} \sim 1.13 \times 10^6$; it results an on axis luminosity of $(5.54 \pm 0.39) \times 10^{51}$

erg s^{-1}. It is really close to the one obtained by Troja et al. 2018 in the case of structured of uniform jets of $\sim 10^{50}$ and also from Granot et al. 2018 $\sim 10^{48.5} - 10^{49.5}$. The errors I obtained account only for the approximation made to evaluate the structured jet light curve, thus they are underestimated considering that also dynamics and emission were approximated and the extremely simplified model.

7. CONCLUSION

Although the proposed model is really simple and quite inaccurate, it results a good first approximation that well describes the main behaviour of the emission from an off-axis jets, with particular attention on the angle of view. The shape of the synthetic light curve for off axis structured jet derived from eqn. 2.55 is promisingly similar, even if it does not properly fits, to the first peak of GRB170817A. The results are in good agreement with more sophisticated models based on accurate hydrodynamical simulations: given an observed luminosity of $(4.9 \pm 0.3) \times 10^{45}$ erg s^{-1} an on axis equivalent of $(5.54 \pm 0.39) \times 10^{51}$ erg s^{-1} is obtained.
Unfortunately, due to the amount of free parameters and the lack of enough known relations between them it is not possible for a model as simple as the presented one to give reliable results. The main issue of the model is to focus on infinitesimally thick emitting regions: this approximation gives a simple expression for the surfaces of equal arrival time, but is quite unrealistic since observation and relations 1.8 and 6.2 suggest a shell thickness of around 10% of R. Secondarily the emission mechanism considered lacks of precision due to the assumption of only synchrotron emission, while also inverse Compton and self-absorption should be considered. furthermore the emission depends strongly on the characteristic of the source, such as emitters density, energy and the magnetic field, quantities whose values are quite uncertain. The model ignores also the dynamics of the ejected material, while this can be an acceptable approximation for the early prompt emission, it is totally unacceptable for later time. Besides a more precise emission mechanism, in order to improve this geometrical model is necessary a more realistic description of both jet's structure and dynamics.

BIBLIOGRAPHY

[1] Abbot et al.,2017, ApJL, 848:L13

[2] Planck collaboration, 2016, A&A, 594, A13

[3] Zhang et al., 2018, Nature Communications, 9:447

[4] Rossi et al., 2002, MNRAS, 332, 945-950

[5] van Eerten et al., 2010, ApJ, 722, 1

[6] Reiss et al. 2016, ApJ, 826, 56

[7] Norris et al. 2005, ApJ, 627, 324

[8] Golkhou et al., 2015, ApJ, 811, 2

[9] Goldstein et al., 2017, ApJL, 848, 2

[10] Granot et al., 2002, ApJ, 570, L61- L64

[11] Granot et al, 2018, MNRAS ,481, 2

[12] Granot et al 2001, GRBs in the afterglow era, ed. E. Costa, F. Frontera, J. Hjorth, Berlin, Springer, 312

[13] Nakar, Sari, 2012, ApJ, 747, 88

[14] van Putten, Della Valle, 2018, arXiv:1806.02165

[15] Rybicki, Lightmann, Radiative processes in astrophysics, New York, Wiley-Interscience, 1979

[16] Lazzati et al., 2017, MNRAS, 471, 1652-1661

[17] Kumar, Panaitescu, 2000, ApJ, 541, L9

[18] Tsvi Piran, 2005, Rev. Mod. Phys., 76, 1143

[19] Troja et al., 2018, arxiv:1801.06516v2